Journal of Aerosol Science 148 (2020) 105584

Contents lists available at ScienceDirect

Journal of Aerosol Science

journal homepage: http://www.elsevier.com/locate/jaerosci

Overview of measurements and current instrumentation for 1–10 nm aerosol particle number size distributions

Juha Kangasluoma [a,b,*], Runlong Cai [b,c], Jingkun Jiang [c], Chenjuan Deng [c], Dominik Stolzenburg [b,d], Lauri R. Ahonen [b], Tommy Chan [b], Yueyun Fu [c], Changhyuk Kim [e,f], Tiia M. Laurila [b], Ying Zhou [a], Lubna Dada [b], Juha Sulo [b], Richard C. Flagan [e], Markku Kulmala [a,b,g], Tuukka Petäjä [b,g], Katrianne Lehtipalo [b,h]

[a] *Aerosol and Haze Laboratory, Beijing Advanced Innovation Center for Soft Matter Science and Engineering, Beijing University of Chemical Technology, Beijing, China*
[b] *Institute for Atmospheric and Earth System Research / Physics, Faculty of Science, University of Helsinki, Finland*
[c] *State Key Joint Laboratory of Environment Simulation and Pollution Control, School of Environment, Tsinghua University, Beijing, 100084, China*
[d] *Faculty of Physics, University of Vienna, 1090, Vienna, Austria*
[e] *Division of Chemistry and Chemical Engineering, California Institute of Technology, 1200 East California Boulevard, Pasadena, CA, 91125, USA*
[f] *School of Civil and Environmental Engineering, Pusan National University, Busan, 46241, Republic of Korea*
[g] *Joint International Research Laboratory of Atmospheric and Earth SysTem Sciences (JirLATEST), University of Helsinki and Nanjing University, Nanjing, China*
[h] *Finnish Meteorological Institute, Erik Palménin Aukio 1, 00560, Helsinki, Finland*

ARTICLE INFO

Keywords:
Aerosol size distribution
Instrumentation
Uncertainty analysis
Review
Sub-10 nm

ABSTRACT

Interest in understanding gas-to-particle phase transformation in several disciplines such as atmospheric sciences, material synthesis, and combustion has led to the development of several distinct instruments that can measure the particle size distributions down to the sizes of large molecules and molecular clusters, at which the initial particle formation and growth takes place. These instruments, which include the condensation particle counter battery, a variety of electrical mobility spectrometers and the particle size magnifier, have been usually characterized in laboratory experiments using carefully prepared calibration aerosols. They are then applied, alone or in combination, to study the gas-to-particle transition in experiments that produce particles with a wide range of compositions and other properties. Only a few instrument intercomparisons in either laboratory or field conditions have been reported, raising the question: how accurately can the sub-10 nm particle number size distributions be measured with the currently available instrumentation? Here, we review previous studies in which sub-10 nm particle size distributions have been measured with at least two independent instruments. We present recent data from three sites that deploy the current state-of-the-art instrumentation: Hyytiälä, Beijing, and the CLOUD chamber. After discussing the status of the sub-10 nm size distribution measurements, we present a comprehensive uncertainty analysis for these methods that suggests that our present understanding on the sources of uncertainties quite well captures the observed deviations between different instruments in the size distribution measurements. Finally, based on present understanding of the characteristics of a number of systems in which gas-to-particle conversion

* Corresponding author. Aerosol and Haze Laboratory, Beijing Advanced Innovation Center for Soft Matter Science and Engineering, Beijing University of Chemical Technology, Beijing, China.
E-mail address: juha.kangasluoma@helsinki.fi (J. Kangasluoma).

https://doi.org/10.1016/j.jaerosci.2020.105584
Received 15 November 2019; Received in revised form 29 April 2020; Accepted 9 May 2020
Available online 30 May 2020

takes place, and of the instrumental limitations, we suggest guidelines for selecting suitable instruments for various applications.

1. Introduction

Sub-10 nm particles form in environments in which vapors transform directly into particles. Molecular clusters first form and subsequent condensation of vapors leads to particle growth. These processes are observed in the atmosphere, high temperature industrial processes, combustion and nanomaterial synthesis. Physical characterization of the product particles is needed to understand all of these systems, but the measurement requirements differ because of the wide range of particle formation and growth rates, as well as number concentrations and particle sizes. For instance, the particle number concentrations may be low in clean arctic environments, requiring extreme sensitivity, but allowing long integration time due to very low precursor concentrations (Wiedensohler, Aalto, Covert, Heintzenberg, & McMurry, 1994), while airborne or roadway measurements may require much faster measurements (Rönkkö et al., 2017; Wehner et al., 2015). Near industrial or combustion sources and even in heavily polluted environments the number concentrations may be too high for many instruments (Tang, Cai, You, & Jiang, 2017). Some laboratory experiments require very high size resolution, but allow e.g. high detection limit and low time resolution (Fernandez de la Mora & Barrios-Collado, 2017). TSI optimal measurement method and instrument therefore varies from one measurement scenario to another as there is no single instrument or method that would fulfill all the prerequisites of a particular application or process.

This paper examines presently available methods and instruments for physical characterization of aerosol particles in the sub-10 nm size regime and offers suggestions regarding instrument choice for different measurement scenarios. We begin with a brief historical perspective that introduces the primary physical characterization methods used for aerosols in this size range as both of the primary methods have been used for over a century. The earliest method for the detection of very small particles involves growing particles by condensation to a sufficient particle size that they can be detected optically. McMurry (2000) provides an excellent review of early developments of this technology. Although initially used to detect larger particles, without reference to size, the expansion cloud chamber was used to study homogeneous nucleation and played an instrumental role in the study of nuclear physics in the early 20th century. Continuous flow instruments that combine condensational activation with optical detection, called condensation particle counters (CPCs), were developed around 1970–1990 (Agarwal & Sem, 1980; Bartz et al., 1985; Bricard, Delattre, Madelaine, & Pourprix, 1976; Okuyama, Kousaka, & Motouchi, 1984; Sinclair & Hoopes, 1975; Stolzenburg & McMurry, 1991), as were the first approaches to estimate a so-called *Kelvin equivalent diameter* using the threshold vapor supersaturation. The most recent review on the CPCs focusing on solutions enabling sub-3 nm particle detection has been provided by Kangasluoma and Attoui (2019).

The second method for the sizing of sub-10 nm particles involves separation according to their electric mobilities, which is the ratio of the migration velocity of a charged particle to the electric field strength that induces that migration. Condenser analyzers were first used to measure so-called *large ions* in the late 19th century, which included particles in the sub-10 nm size range. The first differential mobility analyzer (DMA) was reported in the early 1920s (Erikson, 1921; see; Flagan, 1998 for a history of these techniques; Rohmann, 1923), and were applied to both laboratory and balloon-borne atmospheric measurements. The immediate predecessor of the commercial DMA, an instrument called the electrical aerosol analyzer (EAA) (Liu & Pui, 1975) revealed the size distribution throughout the submicrometer size range, albeit with large uncertainty.

The measurement capabilities of commercial condensation particle counters and differential mobility analyzers, first introduced in the mid-1970s (Bricard et al., 1976; Sinclair & Hoopes, 1975), began to be pushed into the sub-10 nm size range in the mid-1980s (Agarwal & Sem, 1980; Bartz et al., 1985), opening the door for more extensive study of these very small particles. Winklmayr, Reischl, Lindner, and Berner (1991) introduced the “Vienna” DMA as part of an electrical mobility spectrometer that employed highly sensitive electrometer detection to measure size distributions as small as 3.5 nm. The commercial availability of the ultrafine CPC of Stolzenburg and McMurry (1991) accelerated measurements of atmospheric sub-10 nm particles from the mid-1990s (Covert et al., 1996; Mäkelä et al., 1997; Wiedensohler et al., 1994), enabling quantitative measurement of atmospheric new particle formation that contributes a significant fraction of boundary layer cloud condensation nuclei (Kerminen et al., 2012; Merikanto, Spracklen, Mann, Pickering, & Carslaw, 2009; Spracklen et al., 2008). TSI better understand and quantify its impact in the atmosphere, several groups began developing more accurate instruments and methods for characterizing the onset of the new particle formation process from the molecular sizes around 1 nm (Iida, Stolzenburg, & McMurry, 2009; Jiang, Chen, Kuang, Attoui, & McMurry, 2011b; Kulmala et al., 2007b; Stolzenburg, Steiner, & Winkler, 2017; Vanhanen et al., 2011). These developments made tools available for other subfields of aerosol science, such as combustion and industrial processes (Ahonen et al., 2017; Rönkkö et al., 2017; Tang et al., 2017; Wang et al., 2017).

A number of configurations of these two classes of measurements are currently used to measure size distributions in the low nanometer regime. Size distributions with respect to the Kelvin equivalent diameter are made by varying the supersaturation of the working fluid of the CPC, either by stepping or scanning the supersaturation, S, of a single CPC, or by operating a battery of CPCs in parallel, each at a different supersaturation. The former approach is slow when laminar-flow CPCs are employed by scanning typically the condenser temperature. For example, Wiedensohler et al. (1994) reported a time resolution of 30 min for measuring size distributions by scanning the condenser temperature of a prototype TSI 3025, and Kangasluoma et al. (2016a) estimated a time resolution of 7–10 min for the scanning of the growth tube temperature of the Airmodus particle size magnifier (PSM). However, specific attempts to optimize the time resolution of this method have not been reported. By scanning the supersaturation by varying a specific flow inside a mixing-type CPC (Okuyama et al., 1984), such as the Airmodus PSM (Vanhanen et al., 2011), the instrument can be operated in a

continuous supersaturation scan (SS) to probe the distribution of particles with respect to critical supersaturation, enabling time resolution of the Kelvin diameter size distribution of a few minutes. The CPC battery (CPCb) (e.g. Kulmala et al., 2007a) provides data at fewer sizes, but with far greater time resolution of a few seconds.

Another method for extracting the distribution with respect to the Kelvin diameter is by pulse height analysis (PHA) of the scattered light signals from the ultrafine CPC (Marti, Weber, Saros, Vasiliou, & McMurry, 1996). Since pulse height analysis can be performed on a single particle, the time required for size distribution measurements is limited only by that required to obtain adequate counting statistics, but the size range that can be probed is relatively small. Thus only a few studies have used the PHA CPC (O'Dowd, Aalto, Yoon, & Hämeri, 2004; Sipilä et al., 2009).

A number of different types of electrical mobility spectrometers (EMS) exist. The earliest measurements were made using condenser analyzers (as they were called, not to be confused with condenser of a CPC), such as the Gerdien condenser (Flagan, 1998; Gerdien, 1903), which can be built to efficiently detect even small gas ions, or condensers with segmented collection electrodes (Zeleny, 1900). A modern version of that is the neutral cluster and air ion spectrometer (NAIS), which employs a number of segments (25), each connected to a highly sensitive spectrometer to provide higher mobility resolution than did the early condenser analyzers.

The differential mobility analyzer (DMA) of Knutson and Whitby (1975) was transformed into the differential mobility particle sizer (DMPS) by coupling an electrical mobility separator to a continuous-flow CPC (Fissan, Helsper, & Thielen, 1983; ten Brink, Plomp, Spoelstra, & Vandevate, 1983), dramatically enhancing the size resolution of atmospheric particle size distribution measurements. Wang and Flagan (1990) reduced the time resolution to a couple of minutes in the scanning electrical mobility spectrometer (SEMS; commercialized as the scanning mobility particle sizer, SMPS) by continuously scanning the DMA voltage and counting the particles into time bins. A higher time resolution (down to ~1 s) was achieved by operating a number of DMAs in parallel, each operating at a different voltage and each having its own CPC or electrometer detector (Flagan et al., 1991; Stolzenburg et al., 2017).

A third class of methods that has seen less use in recent years involves particle sizing by diffusion. The diffusion battery (Fuchs, 1962; Wu, Cooper, & Miller, 1989) employs a number of stages in series to successively remove particles of increasing sizes by diffusive loss to screens or capillaries, with particles usually being counted by CPCs. This cumulative, low resolution measurement has seen decreasing use since the introduction of the DMPS and later SMPS, though there has been renewed interest recently (Dubtsov et al., 2017).

Inertial separations have also been employed. The micro-orifice uniform-deposit cascade impactor provided limited resolution in the sub-10 nm size range (MOUDI, Arffman et al., 2014). Fernandez de la Mora and others (Fernandez de la Mora, Hering, Rao, & McMurry, 1990; Hering, Fernandez de la Mora, & Halpern, 1988) demonstrated the possibility of the separation of particles throughout the low nanometer size range and even gas molecules by inertial impaction. This method has, however, seen little use outside of its initial demonstration. The electrical low pressure impactors have also been recently extended to sub-10 nm size range (Arffman et al., 2014).

Mass spectrometers can also make online cluster measurements (Eisele & Tanner, 1993; Jokinen et al., 2012; Junninen et al., 2010; Krechmer et al., 2016; Petäjä et al., 2011; Smith, Moore, McMurry, & Eisele, 2004; Zhao, Eisele, Titcombe, Kuang, & McMurry, 2010) and play an important role in elucidating the chemistry of atmospheric cluster formation below 2 nm. The mass spectrometers used in atmospheric science do not yet have the sensitivity in the 2–10 nm size range that is critical to the survival of newly-formed particles to sizes that can contribute to cloud condensation nuclei (CCN) formation. We do not consider mass spectrometric methods further in this paper, but do note that these instruments are critical to understanding the transition from gases to particles (Ehn et al., 2011; Jen, Hanson, & McMurry, 2015; Jiang et al., 2011c).

Since the other methods have seen little use in recent years, we will focus on EMS and CPCb methods in this review. Both EMS and CPCb methods have their advantages and disadvantages. The EMS can detect only charged particles, for which, at most, only 5% of all sampled particles can be counted because of the low charging states (Fuchs, 1963; Hoppel & Frick, 1986; Wiedensohler, 1988). A relatively accurate particle size classification is achieved with a differential mobility analyzer (DMA), in which only a narrow size band of the particles are selected (Flagan, 1999). In the DMA, the particles also need to go through a voltage transition from the classification voltage to the ground before exiting the DMA, inducing electrostatic losses (Attoui & Fernandez de la Mora, 2016; Cai, Zhou, & Jiang, 2019b). Downstream of the DMA, a CPC or an aerosol electrometer (AEM) is used as a detector. Due to electric noise arising from AEMs, these instruments are usually only suitable for laboratory experiments measuring very high concentrations (Cai, Jiang, Mirme, & Kangasluoma, 2019a). The CPCs have very low noise levels and offer single particle counting, while their applicability is limited by the cut-off at the smallest particle diameters. The cut-off is affected also by the particle and condensing liquid chemical composition when the particle size is smaller than a certain diameter and is close to the cut-off size (Hering et al., 2005; Kangasluoma et al., 2014). With the EMS method, further complications might arise from ions created in the charger. If the supersaturation of the CPC used as the counter in the EMS is high enough, it can also detect a fraction of the charger ions overlapping in mobility space with the smallest clusters. The CPCb and SS method do not require charging, but to achieve accurate sizing, the cut-offs must be accurately known for the specific particle composition in a given experiment, which can be a challenge in many cases. The performance of the CPCs is also limited at very high particle concentrations ($>10^5$ cm^{-3}) due to coincidence in particle counting. In general, the EMS method can have a high detection limit with good sizing accuracy, while Kelvin sizing methods have a lower detection limit but with inferior sizing accuracy. These differences are assessed in detail in this study.

By their nature, systems in which sub-10 nm particles are produced set some challenges to the measurements. Due to the fast diffusion and particle loss to any available surfaces, sub-10 nm particles have short lifetimes and require sufficiently fast-measuring instruments to capture the full dynamics of the particles; and the measurement should take place close to the source to maximize the sampling efficiency. Most, if not all, sub-3 nm particles form from gaseous precursors and their concentrations are much higher than the resulting particle concentrations. As this transition from gas-to-particle phase is a quasi-continuous phenomenon in particle-

size space (Olenius et al., 2018), large gradients in the concentration as a function of the particle size can exist, which sets some requirements for the size resolution and causes uncertainties when the sizing is dependent on the particle composition (Kangasluoma & Kontkanen, 2017).

Accurate measurements of the sub-10 nm particle size distributions must overcome several challenges. Owing to their small size and mass, sub-10 nm particles diffuse very rapidly, so sampling systems must be designed to minimize diffusive losses. Traditional aerosol sampling inlets that employ an impactor and/or diffusion drier to ensure that measurements are made at consistent relative humidity suffer high losses of sub-10 nm particles.

Our goal in this review is to examine the current status of 1–10 nm size distribution measurements. We first describe briefly the general operation principles of the instruments used for sub-10 nm size distribution measurements. Then we present size distributions measured from three different sites representing the state-of-the-art in such measurements. This is followed by a literature review on publications that report measurements of sub-10 nm size distributions using at least two concurrent instruments. After the measurement overview, we discuss the measurement uncertainties. Our aim is to assess the relevant instrumental parameters affecting the measurement accuracy. At the end, with the description of the concentration and sizing uncertainties, we make recommendations on selecting sets of instruments for various applications.

2. Instruments

This section briefly covers the currently-used instruments for the sub-10 nm size distribution measurements and their general characteristics. The technical aspects of the instruments are described in more detail in section 4, while here we note some relevant characteristics of the instruments. The EMS- and CPC-based instruments are the focus of this study (sections 2.1-2.4), while we briefly discuss also the other methods (sections 2.5-2.7) that are capable of sub-10 nm size distribution measurements, but not extensively applied. All discussed instruments are listed in Table 1.

2.1. Condensation particle counter, condensation particle counter battery

Most of the instruments discussed in this manuscript incorporate condensation particle counters (CPCs), because they can count

Table 1
Summary of the instruments.

Instrument	Size classification	Charger	DMA	Detector	Working fluid	Commercialized	Reference
CPCb	Kelvin based			Combination of CPCs with different cut-offs	DEG, butanol, water	Several CPC manufacturers	
PSM	Kelvin based			DEG growth, butanol detection	DEG, butanol	Airmodus	Vanhanen et al. (2011)
DEG SMPS	Mobility analysis	X-ray	TSI 3085 or mini-cyDMA	DEG CPC	DEG, butanol	TSI	Jiang et al., 2011
Half-mini DMPS	Mobility analysis	Radioactive	Half-mini (m) or (p) type	PSM	DEG, butanol		Kangasluoma et al. (2018)
nanoSMPS	Mobility analysis	X-ray	TSI 3086	TSI 3776, 3788	Butanol, water	TSI	
1nmSMPS	Mobility analysis	X-ray	TSI 3086	TSI 3777	DEG, butanol	TSI	
scanning nRDMA	Mobility analysis	X-ray	nRDMA	DEG CPC	DEG, butanol		
NAIS	Mobility analysis	Corona		Electrometers		Airel	Mirme and Mirme (2013)
EEPS	Mobility analysis	Corona		Electrometers		TSI	
DMS	Mobility analysis	Corona		Electrometers		Cambustion	
DMA train	Mobility analysis	X-ray	Grimm DMAs	PSM, 3776	DEG, butanol		Stolzenburg et al. (2017)
Drift tube	Mobility analysis			Kanomax CPC		Kanomax	Buckley and Hogan (2017)
PHA CPC	Pulse height analysis				Butanol, DEG		Sipilä et al., 2009, Kuang et al., 2018
Diffusion battery	Diffusion separation			custom CPC	DBP		Dubstov et al., 2017
DDA	Diffusion separation			TSI 3025, PSM	DEG, butanol		Arffman et al. (2017)
HrELPI	Inertial separation	Corona		Electrometers		Dekati	Arffman et al. (2014)
vSANC	Kelvin based			Expansion chamber	Water, butanol		Pinterich et al., 2016

single particles by first growing the nanoparticles via vapor condensation, and then detecting single enlarged particles by light scattering. Several factors constrain the minimum detectable particle size. The supersaturation attained within the CPC for the particular working fluid employed has to be high enough to activate and grow a particle with its specific composition. The supersaturation that is attained must be below that at which the working fluid will homogeneously nucleate. The particle must also survive transport through the sampling system and instrument flow passages to the point at which it would otherwise activate; diffusional losses increase dramatically with decreasing particle size. Careful instrument design has enabled many current CPCs that were initially designed for sub-3 nm detection to detect some particles as small as 1 nm in size. Thus, measurements of particle dynamics now extend to the size of molecular clusters (Hering et al., 2017; Iida et al., 2009; Jiang et al., 2011b; Seto, Okuyama, de Juan, & Fernandéz de la Mora, 1997; Vanhanen et al., 2011; Wimmer et al., 2013). The CPCs for sub-3 nm measurements are reviewed by Kangasluoma and Attoui (2019). CPCs employing a number of working fluids (butanol, water and diethylene glycol (DEG)) are available from different manufacturers commercially. Their designs span a range of aerosol flow rates, cut-off diameters, and response times; these parameters can be tuned by the user within some limits. The technical details for specific CPCs are discussed further in section 4.

A battery consisting of two or more CPCs (CPCb) that are operated in parallel without upstream size selection is the most straightforward method for acquiring size distribution data, though not necessarily the easiest to interpret. The simplest assumption is to assume that the concentration difference between two CPCs with different size-dependent response functions can be described in terms of the particle size that is counted with 50% efficiency, d_{50}, and assuming that all particles larger than that size are counted while no smaller ones are detected. The counting efficiency of most CPCs rises from zero to its maximum value over a wide size range so this simplistic analysis is a poor approximation. Moreover, the size dependent counting efficiency depends upon the compositions of the particles being sampled and may thus vary with time during the course of an experiment. With multiple CPCs, the inversion procedure should take into account the shape of the collection efficiency curves at each instant of time in the measurement (Fiebig, Stein, Schröder, Feldpausch, & Petzold, 2005). This level of analysis requires detailed calibration of each of the CPCs with particles of appropriate composition and entails solving a typical ill-posed data inversion problem.

The clear advantages of the CPCb are its fast response and its sensitivity toward low particle concentrations since all particles can be counted, not just charged ones. The time response is limited only by the sampling flow smearing in the sampling line, the response time of the CPCs and random fluctuations in the measured particle concentrations. Size distribution measurements with the CPCb using commercially available CPCs can attain 1–2 s time resolution. The number of CPCs in the battery and the shape and composition-dependence of the detection efficiency curves are the primary factors limiting its size resolution.

2.2. Supersaturation scan

Several mixing-type CPCs that are capable of detecting 1 nm particles while scanning the supersaturation have been reported (Gamero-Castano & Fernandéz de la Mora, 2000; Kim, Okuyama, & de la Mora, 2003; Kim et al., 2002; Seto et al., 1997; Sgro & Fernandéz de la Mora, 2004; Wang, McNeill, Collins, & Flagan, 2002). However, only one of them is currently commercially available as a supersaturation-scanning CPC - the Airmodus A11.

The Airmodus nano condensation nuclei counter (nCNC, model A11) is a two-stage CPC, consisting of a mixing-type particle size magnifier and a separate CPC (Vanhanen et al., 2011). The instrument is commonly called a particle size magnifier, PSM. We use this name as it is commonly used in our field. In the instrument, the inlet flow rate of 2.5 L per minute (lpm) is mixed in a T-shaped mixing piece with a 0.1–1.3 lpm flow rate that is saturated with diethylene glycol (DEG). The mixed flow is brought to a condenser where the peak supersaturation takes place, activating the particles and growing them to about 100 nm in diameter. The particles grown by DEG in this first stage are transported to a CPC downstream of the condenser; the CPC further grows the droplets to detectable sizes with butanol as the working fluid. Varying the DEG-saturated flow rate changes the peak supersaturation in the condenser, thereby altering the cut-off diameter. Size-resolved particle concentrations are determined with several different inversion methods with d_{50} values spanning the 1–3 nm range and with a resolution of approximately 1.5–5 ($Z_p/\Delta Z_p$) (Cai et al., 2018b; Lehtipalo et al., 2014). With current hardware and inversion routines, the time resolution of the PSM is 2 min. The dependence of DEG-based particle detection and sizing on the particle chemical composition and its related uncertainties are discussed more in detail in section 4. It should also be noted that the inversion of the supersaturation scan method, which is a cumulative method, is more sensitive to air mass fluctuations than the differential methods, such as the SMPS.

2.3. Electrical mobility spectrometers

Three types of electrical mobility spectrometers are presently being used for sub-10 nm size distribution measurements. With traditional SMPS or DMPS instruments, the particles are brought to a steady-state charge distribution by exposure to bipolar gas ions in a charge conditioner, size selected with a mobility classifier, and counted with a one- or two-stage CPC (Wang & Flagan, 1990; Wiedensohler et al., 2012). A number of different classifiers are used to enable sizing below 10 nm. These include the TSI nanoDMA 3085 (Chen et al., 1998) and its modification, model 3086 (Stolzenburg, Scheckman, Attoui, Han, & McMurry, 2018), for better size resolution, short Vienna-type DMAs (Winklmayr et al., 1991) and its derivatives, e.g., the (p) and (m)-type Half-mini DMA (Fernandéz de la Mora, 2017; Fernandéz de la Mora & Kozlowski, 2013) and the mini-cyDMA (Cai, Chen, Hao, & Jiang, 2017a). Owing to the sizing limits, the TSI nanoDMA and short Vienna-type DMAs are typically paired with a TSI ultrafine CPC to enable measurements down to 3 nm diameter. To enable measurements down to 1 nm in diameter, the modified TSI 3086 DMA, the SEADM Half-mini (m) DMA, or the mini-cyDMA have been paired with a two-stage DEG-based CPC, with the first stage being either a laminar-flow CPC, or a mixing type CPC, such as the PSM (Cai et al., 2017b; Jiang et al., 2011b; Kangasluoma et al., 2018). Typical DMPS or SMPS systems operate at a

time resolution of minutes, while SMPS operation with a time resolution in the order of some seconds has also been demonstrated in laboratory conditions (Tröstl et al., 2015; Wang et al., 2002).

If higher flow rates can be tolerated, or if measurements include high-concentration aerosols, a Faraday cage electrometer can be used as the detector instead of a CPC in the second class of instruments, as is done with ion spectrometers (e.g. Electrical Aerosol Spectrometer (Tammet, Mirme, & Tamm, 2002), Air Ion spectrometer AIS (Mirme et al., 2007), Balanced Scanning Mobility Analyzer, BSMA (Tammet, 2006), or Scanning Inclined Grid Mobility Analyzer, SIGMA (Tammet, 2011)) that can measure ions down to 1 nm. The ion spectrometers measure naturally-charged ions without external charging. This technique has been also modified for size distribution measurements by adding a unipolar corona charger prior to ion distribution measurement, as seen in the Neutral cluster and Air Ion Spectrometer (NAIS) (Mirme & Mirme, 2013) and in the Engine Exhaust Particle Sizer (Johnson, Caldow, Pöcher, Mirme, & Kittelson, 2004), which are limited in the lower size to around 2 nm and 6 nm, respectively. The time resolution of the ion spectrometers is typically in the order of minutes in their normal measurement cycle, while operation at around 1 s time resolution is possible.

Fast-response electrical mobility size distribution data can be obtained by operating a number of DMAs in parallel, each paired with a CPC or an electrometer detector. With each DMA set to continuously monitor a different particle size, the time resolution is limited only by the inherent time response of the DMA-CPC or DMA-electrometer combination (Flagan et al., 1991). While that time response is somewhat slower than that of the CPC itself (Mai, Kong, Seinfeld, & Flagan, 2018), and care must be taken to account for the different time responses of the different DMA-detector pairs, the time resolution is much faster than is possible with conventional DMPS or SEMS/SMPS measurements. The gain in time resolution is most pronounced in environments of low signal, since each CPC is accumulating counts at a fixed size.

2.3.1. DEG SMPS, half-mini DMPS, nanoSMPS, scanning-mode nRDMA

The DEG SMPS generally refers to an SMPS that employs a TSI ultrafine CPC as the detector that is modified to operate with DEG and uses another butanol CPC to count the droplets (DEG CPC). The DEG CPC was later commercialized by TSI as the 3077 nanoEnhancer, and when coupled to their soft x-ray charger and 3086 DMA, as the 1 nm SMPS. For the measurements reported in this review, the DEG SMPS includes a core sampling system to increase the particle transmission efficiency from the atmosphere to the charger inlet (Fu, Xue, Cai, Kangasluoma, & Jiang, 2019; Kangasluoma et al., 2016a), a commercial TSI X-ray charge conditioner (model 3088) (Jiang et al., 2014), and a mini-cyDMA that has been optimized for high penetration and high size resolution SMPS measurements (Cai et al., 2017a). The CPC consists of a TSI 3776 that has been modified in the following ways: 1) the saturator wick is replaced with one that is suitable for DEG; 2) a Nafion dryer is added into the sheath flow to remove water; 3) the tunable range of the saturator temperature has been extended; 4) the aerosol and sheath flow rates have been increased to 0.1 and 0.9 lpm, respectively. These improvements have increased the sensitivity of the DEG SMPS by a factor of approximately 5–10, depending on the particle size (Cai et al., 2019a).

The Half-mini (HM) DMPS is another prototype EMS consisting of a core sampling system, radioactive charger, a SEADM Half-mini DMA as a classifier (Fernandéz de la Mora, 2017), and the PSM as a detector. The system has been described and characterized by Kangasluoma et al. (2018). The total particle penetration in the DEG SMPS is slightly higher than that of the Half-mini DMPS because the penetration in the DMA is higher, and the DEG SMPS does not require a flow split between the DMA and the CPC (Cai et al., 2019a). On the other hand, the aerosol flow rate that is counted in the CPC of the Half-mini DMPS is larger (see section 4.1), resulting in almost identical statistical uncertainties. As a result, the two instruments attain similar overall performance in the size distribution measurements below 10 nm.

By TSI nanoSMPS, or nanoSMPS, we refer to a commercial SMPS from TSI that is based on a TSI aerosol charger, the TSI nanoDMA and one of the various models of TSI ultrafine CPCs. Within this review we don't differentiate between the specific components of the SMPS, i.e., we assume that each combination of their instruments produces the same size distribution, which might not be true close to 3 nm where the CPC detection efficiency can vary depending on the CPC. The SMPSs typically detect only particles larger than about 3 nm in diameter, because the CPCs that have been used are TSI ultrafine CPCs, but not the DEG-based nanoEnhancer (Model 3777). Based on the prototype DEG SMPS by Jiang et al. (2011b), TSI has recently introduced a 1 nm SMPS (3938E57), with a newly-modified nanoDMA (3086) and DEG-based CPC (3757) (Betrancourt et al., 2017) to which we did not have access at the time of the experiments reported in this paper.

The nano radial DMA (nRDMA) designed by Brunelli, Flagan, and Giapis (2009) was coupled with a two-stage DEG CPC for scanning size distribution of the sub-10 nm particles with a 2 min time resolution. The nRDMA has also been characterized by Jiang et al. (2011a). For the two-stage detector, small-sized custom laminar flow DEG saturator and condenser were made and deployed together with a TSI butanol CPC (3760A, cut-off of 11 nm) in series, which allowed to detect particles as small as 1 nm. A custom-made soft X-ray charger with a Hamamatsu 4.9 keV soft X-ray emitter was also designed with a short residence time (less than 2 s) for minimizing diffusion loss through it. Because positive high voltage (up to 5 kV) was applied to the nRDMA for classifying positively-charged sub-10 nm particles in scanning-mode, a high-throughput DMA inlet based on the design of Franchin et al. (2016) was used to minimize the particle loss due to the sudden potential jump between the outlet of the soft X-ray charger and the inlet of the radial DMA by smoothing the potential gradient.

The performance of the SMPS- and DMPS-systems reported here is affected by the low charging efficiency of bipolar charge conditioners in the sub-10 nm size range and by particle losses within the DMAs. The size distributions are, therefore, inferred from relatively low particle counts. Furthermore, some uncertainty exists in the bipolar charged fractions in the sub-10 nm size range.

2.3.2. Neutral cluster and air ion spectrometer (NAIS), engine exhaust particle sizer (EEPS), differential mobility spectrometer

The Neutral cluster and Air Ion Spectrometer (NAIS, Mirme & Mirme, 2013) is an electric mobility spectrometer consisting of two mobility classification columns, one for each polarity. The NAIS takes a large sample flow rate of 54 lpm, and splits it between the two channels. The particles are first discharged with a corona needle, after which the primary charging takes place with another corona needle. The particles obtain a unipolar charge distribution. The charged particles are brought to a DMA column, of which the inner electrode consists of a series of 25 electrometers measuring the electric current carried by the particles. The NAIS measurement size range for particles is 2–40 nm and 0.8–40 nm for ions, and its size resolution is around 2.8 at 1.47 nm. The inherent problem with the aerosol measurements in the small size range arises from the use of corona charging and subsequent electrical detection. The excess ions produced by the charger are filtered prior to sizing, but some of them penetrate into the DMA. This signal cannot be distinguished from the charged aerosols in sub 2 nm sizes (Gagne et al., 2011). However, with the high aerosol flow rate and long integration time for each size bin due to the use of multiple electrometers, the concentration detection limits of the NAIS can be similar or lower than the current SMPS/DMPS systems (Cai et al., 2019a).

The operation principle of the engine exhaust particle sizer (EEPS, TSI) and the differential mobility spectrometer (DMS, Cambustion) is similar to the NAIS: a unipolar charger combined with a DMA column with positive voltage in the central electrode, and a series of electrometers at the outer walls. The EEPS and DMS have been mostly utilized in the field of emission studies.

2.3.3. DMA train

The DMA train reported in this study is that designed by Stolzenburg et al. (2017). The DMA train uses six parallel Grimm DMAs (Jiang et al., 2011a) paired with CPCs in order to enable high sensitivity, good counting statistics, and excellent time resolution during sub-10 nm size distribution measurements. TSI channels for the smallest particle sizes use the combination of the Airmodus A10 and TSI 3772 (previously TSI 3776) downstream of the DMA, while the other four use the TSI 3776 CPC. With the published configuration, the DMA train reaches either fast time response time or extremely low limits of detection due to parallel sizing and detection scheme.

2.3.4. Drift tube ion mobility spectrometer

Electrical mobility analysis of charged particles can also be conducted in counter flow drift tubes. Such an analysis method requires a fast detector to separate ions of different flight times at the end of the drift tube. A combination of a drift tube and a CPC has been designed and first measurements reported by Oberreit and coworkers (Oberreit et al., 2015; Oberreit, McMurry, & Hogan, 2014a; b), and the instrument is characterized more completely by Buckley and Hogan (2017). The instrument uses bipolar charging upstream of the drift tube and a fast CPC as the detector downstream of the drift tube. They have used the instrument mainly for laboratory characterization of nanoparticle dynamics (Oberreit et al., 2015; Oberreit et al., 2014a; b; Ouyang, He, Larriba-Andaluz, & Hogan, 2015).

2.4. Pulse height analysis CPC

The size analysis in the pulse height analysis (PHA) CPC is based on the observation that smaller particles start growing at a higher supersaturation inside the CPC condenser than larger particles, thus having less time for the condensational growth. The light intensity scattered from the grown particle is dependent on their size, and therefore there is a link between the initial particle size and the final droplet, which can be detected using the PHA technique (Dick, McMurry, Weber, & Quant, 2000; Marti et al., 1996; Saros, Weber, Marti, & McMurry, 1996). Sizing by the PHA is limited to very small particles (<10 nm or less depending on instrument), where there is a clear time difference in their activation in the condenser. The PHA CPCs have been modified also for detecting sub-3 nm particles by increasing the supersaturation to levels at which homogeneous droplet formation occurs (Kuang, 2018; Sipilä et al. 2008, 2009). Challenges related to the PHA CPC are that the size resolution is relatively low, the sampled concentration should be low, and the response is sensitive to particle chemical composition.

2.5. Diffusion battery, differential diffusion analyzer

Diffusion-based instruments perform sub-10 nm particle sizing based on the high diffusivity of the particles. The size separation with diffusion batteries is typically done by bringing the aerosol flow through different number of screens onto which particles diffuse according their diffusivity. The size distribution is measured by varying the number of diffusion screens the aerosol flow passes through. As part of a workshop reported by Wiedensohler et al. (1994), the diffusion battery was for the first time extended to sub-10 nm particle sizing. They used 10 diffusion screens from TSI, and used the TSI 3025 as the detector. Recently, Dubtsov et al. (2017) also demonstrated the usability of a screen-type diffusion battery down to 3 nm. In that instrument, there are eight screen stages, after which a mixing type CPC grows the particles using dibutylphthalate, and counts the particles optically.

The first differential diffusion analyzer (DDA) was constructed by Arffman, Juuti, Harra, and Keskinen (2017). The design of that instrument is such that the aerosol flow is brought to a flow mid-plane with sheath flow around it in a planar geometry. The particles diffuse toward the outer walls, in which a small slit extracts particles of a given diffusivity range. The mean particle size that is extracted can be varied by changing the aerosol-to-sheath flow ratio. Arffman and coworkers report on the characterization of the instrument, while applications of the DDA have not yet been reported.

2.6. High resolution low pressure impactor

Electrical low pressure impactors (ELPI) are instruments in which particle size classification is obtained via a cascade of impactors with varying aerodynamic cut-off sizes (Keskinen, Pietarinen, & Lehtimäki, 1992). Prior to the impactor stages, the particles are charged with a unipolar corona charger and the particle detection is achieved by placing an electrometer at each impactor stage. This instrument has been tuned for sub-10 nm particle detection by improving the impactor nozzles, which provides discrete cut-off curves (Arffman et al., 2014).

2.7. Expansion CPC

Based on the expansion CPC of the aerosol physics Vienna group (Winkler et al. 2004, 2008), a portable version of that instrument was constructed by Pinterich et al. (2016). The working fluid in the vSANC can be water or any alcohol that is evaporated to the sample flow via a cylindrical humidifier. The saturated sample flow is brought to the expansion chamber, which is operated semicontinuously. Size distributions are measured by varying the supersaturation, resulting from the expansion by varying the expansion ratio.

3. Atmospheric and chamber measurements

To obtain insight into how accurately we can measure sub-10 nm particle number size distributions, we analyzed measurements from three different sites, Hyytiälä, Beijing and the CLOUD (Cosmics Leaving OUtdoor Droplets) chamber at CERN (European Organization of Nuclear Research), which we consider to be among the state-of-the-art for sub-10 nm particle measurements. After that, we collected a literature review on the published measurements, in which at least two instruments were measuring the same aerosol regardless of whether the purpose of the study was a technical, atmospheric or methodological study.

3.1. Sub-10 nm particle size distribution measurements

For the atmospheric data, we plotted two types of data: median distributions that were measured over a long time period and hourly median distributions. We define the median size distribution such that it is the size distribution given by median dNdlog/Dp value at each size during the specified time period. Measuring the median distributions over long time periods makes it possible to assume that the variations in the instrument operation and sample properties average out, so the comparison should reflect the average instrument performance. The hourly particle size distribution plots reveal cases in which the measurement can be more influenced by the atmospheric fluctuations, and by sample and particle properties. The accuracy of these measurements is put into scope in section 3.2.

3.1.1. Clean boreal atmosphere, Hyytiälä SMEAR II-station

In Hyytiälä, Southern Finland at the Station for Measuring Ecosystem – Atmosphere Relations II (SMEAR) (Hari & Kulmala, 2005), an ultrafine DMPS (a combination of a radioactive charger, a Hauke-type DMA and a TSI 3025A or 3776 ultrafine CPC), a NAIS, and a PSM measured the atmospheric particle size distributions continuously since 1996, 2006 and 2014, respectively (Aalto et al., 2001; Kontkanen et al., 2017; Manninen et al., 2009). During spring 2017, a Half-mini DMPS was also introduced for a one month-long campaign to allow for a comparison with the long term instruments. Kangasluoma et al. (2018) reported a comparison of the Half-mini DMPS and ultrafine DMPS, mostly focusing on instrumental aspects of the DMPS systems and counting related uncertainties. The DMPS was sampling through the roof of a cottage at a height of about 8 m. The NAIS sampled directly through the wall of the same cottage with a ~50 cm long sampling line. The Half-mini DMPS was located in a nearby container about 10 m away from the other two instruments, sampling with a core sampling inlet with a 50 cm sampling line. The long-term PSM employed a similar core sampling system as the Half-mini DMPS, and was located next to it in the same container. We assume the possible local fluctuations in the particle concentrations average out over the one-month period, and that the presented distributions reflect variations in the instrument

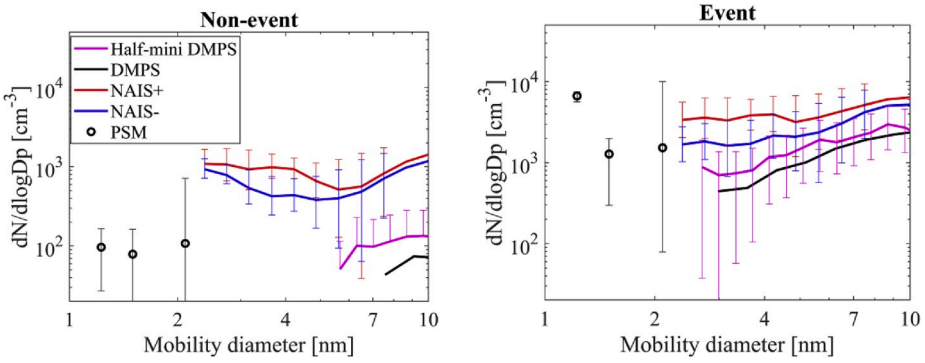

Fig. 1. Median size distributions over three weeks in May 2017 measured in Hyytiälä for non-event and event days. Measured particle polarity is given in the legend.

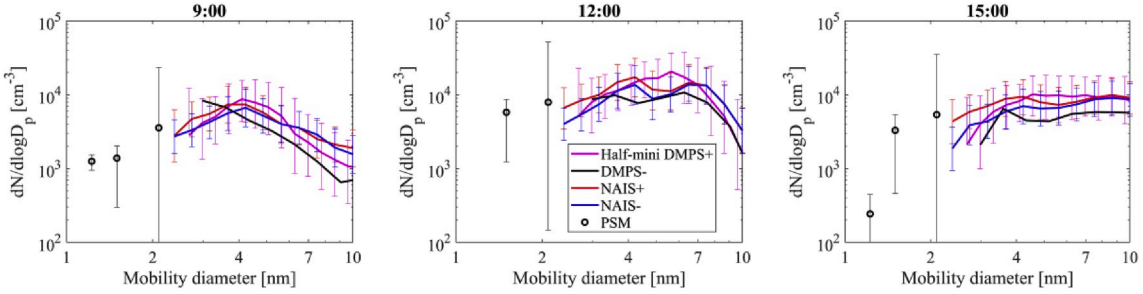

Fig. 2. Hourly median size distributions in Hyytiälä on an event day May 7, 2017 at 9, 12 and 15. Measured particle polarity is given in the legend.

response to the same atmospheric size distributions. More details of the study can be found in Kangasluoma et al. (2018).

Fig. 1 shows the median size distributions over three weeks from the same data set for the four instruments. The data are separated into new particle formation event days and non-event days so that we may observe the instrument performance at times with high and low sub-10 nm particle concentrations. The errorbars are determined using the method described in section 4.5, and a Matlab functions used to calculate them are given in the supplementary material. In Figs. 1–5, errorbars are plotted for selected instruments (Half-mini DMPS, DEG-SMPS, PSM, NAIS) typically used for sub-10 nm size distribution measurements. It is important to note that the errorbars represent uncertainty for a single measurement, and do not include variation in the data.

During event times, the NAIS detected a size distribution function in which the number concentrations in the 3–10 nm size range were a factor of 2–8 higher than those measured by the two DMPS systems. Although the PSM did not overlap in size with the DMPSs, the trend in the size distribution function was of the same order of magnitude as those detected by the DMPS systems. The Half-mini DMPS did not detect particles below 2.7 nm in size, probably because newly-formed particles in the boreal forest environment consisted of oxygenated hydrocarbons for which the cut-off of DEG based CPCs was in the range of 2–3 nm at supersaturation that did not produce homogeneously-formed DEG droplets (Kangasluoma et al., 2014). The scanning PSM, on the other hand, is operated at higher supersaturation, with background correction for homogeneously nucleated droplets, which is why it can detect particles also in the sub-3 nm size range. During non-event times, the median particle concentrations in the size range of 1.5–6 nm were below the detection limit of the PSM, DMPS and the Half-mini DMPS, while the NAIS reported a size distribution function in the range of 10^3 $dN/dlogD_p$, which might be related to the inversion of the instrument. At around 10 nm, the NAIS reported a size distribution function of about a factor of 10 larger than the DMPSs (Manninen et al., 2009).

Fig. 2 presents the instrument response on an NPF day May 7, 2017 with three hourly median distributions at 9:00, 12:00 and 15:00 for the evolving size distributions. Note that concentration of one data point at 12:00 is smaller than the y-axis minimum value. At 9:00, the mode diameter appeared at around 4 nm and particles grew such that the mode diameter at 12:00 was about 6–7 nm, while it was about 10 nm at 15:00. The instruments exhibited quite a good agreement during this day, with the largest discrepancies being about a factor of 10 at 2–3 nm.

3.1.2. Urban megacity, Beijing

Continuous measurements were established at the Beijing University of Chemical Technology (BUCT) west campus inside urban Beijing in the beginning of 2018 (Zhou et al., 2019). For the long-term sub-10 nm size distribution measurements, the station operated a PSM, NAIS and DMPS, and also for our selected measurement period an SMPS, which was a combination of the DEG SMPS (1–6 nm) (Cai et al., 2017a; Jiang et al., 2011b) and a Tsinghua University-operated twin-SMPS (6–1000 nm) (Liu, Jiang, Zhang, Deng, & Hao, 2016) using a TSI x-ray neutralizer and combinations of a TSI 3085 nanoDMA, a TSI 3776 ultrafine CPC and a TSI 3081 DMA with a TSI 3772 CPC, in order to cover the whole size range from 1 nm to 1 μm. The instruments were located on 5th floor of the building, sampling either through a window (PSM, NAIS, DEG SMPS) or from the roof (Tsinghua twin-SMPS). The PSM was sampling with a core sampling system with a 1.3 m line. The NAIS sampling line was about 1 m long, and was located next to the PSM. The DMPS sampled with a 2.5 μm preimpactor and drier in the sampling line and covered the size range of 6–840 nm with a single DMA by measuring in two flow modes with a TSI 3772 as the detector. Thus, the DMPS was not fully optimized for the sub-10 nm size range and we do not discuss its data here. The DEG SMPS was positioned about 5 m away from the PSM and the NAIS; it also employed core sampling.

From the data, we identified two characteristic types of days, namely those affected by haze (with a high mass concentration of fine particulate matter) and new particle formation (NPF) event days (with a high number concentration of ultrafine particles followed by their growth towards larger sizes). As the corresponding size distributions were very different, we separated the data accordingly. We selected 14 days with NPF event and 31 haze days in 2018 for the comparison. As we did for Hyytiälä, median and hourly size distributions are presented for one day. In Beijing, we expect that the 1–2 nm particles are mostly consisting of acid-base clusters such as sulfuric acid-dimethyl amine (Yao et al., 2018), while at larger sizes, oxygenated organics also participate in particle formation but the exact particle compositions at each size are unknown. We can make the following observations from Fig. 3: during NPF, the NAIS consistently detects a different shape distribution than the DEG SMPS with seemingly very characteristic crossover around 3 nm, while the DEG SMPS and the PSM agreed within a factor of 3. The trends in the measured size distributions agreed quite well. Based on the discussion on the sources of uncertainties in these measurements, this agreement between the PSM and DEG SMPS can be considered fairly good. During haze events, the DEG SMPS lacked the sensitivity to detect particles below 3 nm, while the PSM still reported

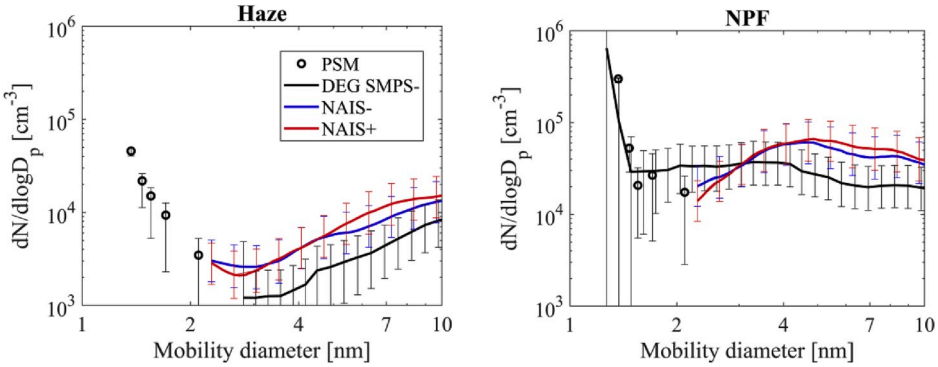

Fig. 3. Median size distributions over selected haze or NPF days during 2018 measured in Beijing.

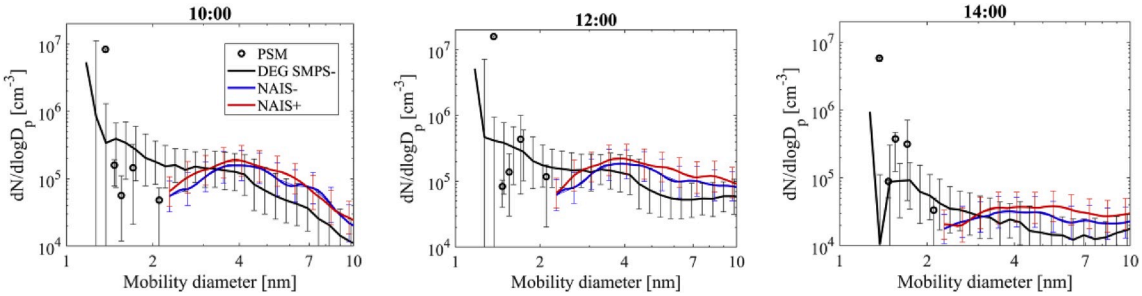

Fig. 4. Median hourly size distributions on an NPF day December 25, 2018 measured in Beijing. Measured particle polarity is given in the legend.

elevated sub-3 nm particle concentrations. The interesting observation of persistent existence of sub-3 nm particles, even during times when the condensation sink is high, also shown in Zhou et al. (2019) and Chan et al. (2020).

Fig. 4 compares size distributions from a new particle formation event day on December 25, 2018 at 8, 12 and 14 o'clock. As in Fig. 3, in all cases, the NAIS detected different shape of the size distribution than the DEG SMPS: higher number concentrations above 3 nm, and lower number concentrations below 3 nm by a factor of 1–5. Especially in the morning, but also throughout the day, the PSM detected size distribution functions similar to the DEG SMPS. Depending on particle size and measurement time, the PSM data can overestimate or underestimate the concentrations measured by the DEG SMPS by a factor of more than 10. One possible cause for this discrepancy could be that the particle composition changes with time such that they are more easily activated earlier in the day. Another possibility was that the charging efficiency decreased strongly because of the changing particle composition or charger ion composition (Chen, McMurry, & Jiang, 2018; Chen & Jiang, 2018; Premnath, Oberreit, & Hogan, 2011). Last, it is possible that changes in the air masses are frequent enough to cause uncertainties of different magnitudes to the concentrations inverted from the raw data of the PSM and the DEG SMPS.

3.1.3. CLOUD

A PSM, DMA train, NAIS, scanning-mode nRDMA and nanoSMPS (with an ultrafine water CPC) measured particle number size distributions in the CLOUD chamber operated at CERN, Switzerland. For our study, we selected three experiments from CLOUD campaign 12, which ran from September–November 2017. The test aerosol was produced by nucleation by three different mechanisms: from oxidation of pure alpha-pinene with ozone at 5 °C, from oxidation of a mixture of sulphur dioxide and anthropogenic organics (AVOCs): toluene, trimethylbenzene and naphthalene by the hydroxyl radical at 20 °C, and from iodic acid vapor, typical for marine environments. For our purposes, the most important difference between the experiments is the resulting particle composition. The chamber has been discussed in detail elsewhere (Duplissy et al., 2010; Kirkby et al., 2011), so a more detailed description of the chamber and its operation is not necessary here. All instruments were placed around and as close as possible to the chamber. The PSM was sampling together with three other PSMs from the same port. The flow was split to all PSMs using a double-T split, and its particle losses in the line were experimentally characterized to correct the data. The NAIS sampled at one port together with the Cluster Ion Counter. The DMA train sampled at 20 lpm using core sampling through a 1-inch port at the opposite end of the well-mixed chamber compared to the PSM and NAIS ports. The nanoSMPS and scanning-mode nRDMA were located next to the DMA train and shared 10 lpm from a core-sampler using a custom-made Y-splitter (1.5 and 4.6 lpm, respectively, with excess of 3.9 lpm for reducing diffusion loss during the core-sampling).

Fig. 5 presents hourly median size distributions measured by the five instruments for each of the three experiments. The time periods selected were ones in which the chamber had reached steady state, so the size distribution was relatively stable, and should

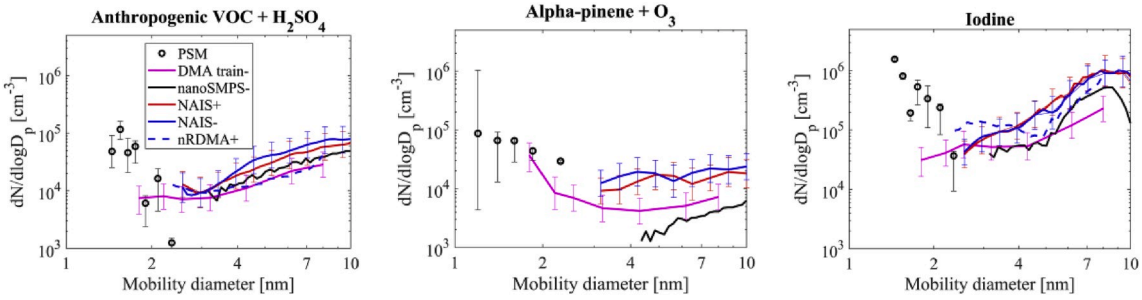

Fig. 5. Median size distributions over 1h measured in the CLOUD campaign. Measured particle polarity is given in the legend.

allow good instrumental comparison. Particle number size distributions from AVOC and iodine experiments were qualitatively similar: they were bimodal, such that one peak remained below 2 nm and another one resided around 10 nm. In both cases, the instrumental agreement was within a factor of about 10; discrepancies being larger below 3 nm while around 10 nm the instruments agreed slightly better. The size distributions from the alpha-pinene oxidation experiment showed no clear peak below 10 nm. The nRDMA was unavailable during the alpha pinene experiment. The instrumental agreement was similar to that of the other two experiments, except that the water CPC based nanoSMPS exhibited clearly lower size distribution functions than the NAIS or DMA train. This was most likely due to inability of the water CPC to activate these specific organic compounds, which, interestingly, was not observed for the AVOC experiment, where also sulfuric acid was present.

3.2. Site summary

The measurements from the three sites reveal that the agreement between the different instruments is relatively good when the data is averaged over a long period of time. Long averaging possibly also averages out some instrumental discrepancies observed in the hourly plots. Generally, the NAIS typically reports larger concentrations than do the other EMSs; this difference was especially pronounced in Hyytiälä during non-event days. In many cases, the PSM also reports a higher size distribution function than the closest EMS, but the comparison is more difficult since there is often not enough overlap in the size ranges. Measurements in the size range of 1–3 nm are subject to large uncertainties due to differences in the PSM sizing mechanism, uncertainties in the charging probability and the CPC detection efficiency in the mobility-based instruments. Note that the population of sub-3 nm particles during NPF events in Beijing is significantly higher than that in Hyytiälä and is also higher than some of the CLOUD experiments. It certainly benefits the measurement.

This glimpse into the current state-of-the-art sub-10 nm size distribution measurements suggests that the instrumental agreement in the 3–10 nm size range is relatively good, in most cases agreeing within a factor of 5, and the size distribution functions trends agree qualitatively. Below 3 nm, measurements are much more challenging due to the many subtle features that affect the measurement accuracy. These are discussed in the sections below. Instrumental comparisons using atmospheric data especially in this size range would be very beneficial. Ideally, at least one EMS and PSM should be used, preferably two or more, and the instruments should be operated and maintained by independent research groups.

3.3. Literature review

To obtain an overall picture on the accuracy of the sub-10 nm particle size distribution measurements, and especially how well individual measurement methods and instruments agree or disagree with each other, we review the past efforts in intercomparing size distribution measurements. When a factor between the instruments or concentrations is discussed in this section, it refers to the approximate multiplier between the lowest and highest measured concentration in the worst comparison.

The first field intercomparison was conducted very early after the publication of the first ultrafine particle counter of Stolzenburg (Stolzenburg & McMurry, 1991) by Wiedensohler et al. (1994), who compared four independent methods for sub-10 nm particle size distribution measurements, including: an ultrafine DMPS, an ultrafine diffusion battery, a PHA CPC and a temperature-scanning ultrafine CPC. Their comparison of the size-resolved particle concentrations, and the 3–10 nm particle concentration show agreement, within a factor of approximately 1–5 and 1–3, respectively. This agreement can be considered extremely good, especially given that they were comparing early prototype instruments. Indeed, in the scope of the following review, the results are very impressive. Further, such dedicated and extensive workshops or intercomparisons of different sub-10 nm size distribution measurement techniques have not been repeated since that pioneering study.

A field comparison of an ultrafine DMPS against a CPC pair with cut-offs of 3 nm and 10 nm, and a PHA CPC against the same DMPS for sub-6 nm particles was reported by Aalto et al. (2001). The CPC pair detected particle concentrations of around 2–5 times more than did the DMPS, while the DMPS recorded concentrations about 10–15 times larger than the PHA CPC. Lehtipalo, Sipila, Riipinen, Nieminen, and Kulmala (2009) and Lehtipalo et al. (2010) reported comparisons of the NAIS and PHA CPC in the size range of 1.5–3 nm and 3–5 nm measured in Hyytiälä and in Mace Head, respectively. In the former, the NAIS detected larger particle concentrations than the PHA CPC when the concentrations were relatively high (e.g., day time), while the opposite was true for low particle

concentrations. In the latter, the NAIS reported consistently larger concentrations than that of the PHA CPC. Manninen et al. (2009) compared the NAIS and DMPS in Hyytiälä for the particle size range of 3–20 nm. Almost without exception, the NAIS detected concentrations at least 2 times larger than the DMPS. When the concentration detected by the DMPS was in the range of hundreds per cm^3, the difference in the detected concentrations was sometimes even larger than an order of magnitude. Kulmala et al. (2007b) compared two prototype ultrafine CPCs (Mordas, Sipila, & Kulmala, 2008), with cut-offs of 1.8–3 nm, against measurements in that size range made using the NAIS. The instruments agreed relatively well during times of new particle formation, while evening and morning concentration ratios exceeded 10 or more at times, with the NAIS detecting more particles.

Wiedensohler et al. (2012) published results from a large Aerosol, Clouds and Trace Gases Research Infrastructure (ACTRIS) DMPS workshop that focused on the overall performance of the DMPS systems, which included highly interesting results from simultaneous measurements of sub-20 nm size distribution measurements. The size distributions from the inversion of simultaneous atmospheric measurements from seven DMPS systems showed significant disagreement in the vicinity of 10 nm, with dN/dlogDp varying from 0 to 4500 cm^{-3}. These results are especially relevant to cases in which sub-20 nm aerosol dynamics or other properties are inferred from the data measured by "conventional" DMPS systems. A smaller intercomparison of two DMPS systems has been reported by Kangasluoma et al. (2018), who constructed a DMPS system based on a Half-mini DMA and a Airmodus PSM. In that comparison, the new Half-mini DMPS detected concentrations that exceeded those of other DMAs by a factor of 2.2 to 1.2 over the 3 nm–10 nm size range. Their analysis also included estimates of the statistical uncertainties originating from the counting; the size classified particle concentration uncertainties from the new DMPS were about half for those from the long-term monitoring DMPS due to the higher sample flow rate (0.71 lpm in the PSM of the Half-mini DMPS vs. 0.05 lpm in the 3776 of the DMPS). Measurements of soot formation in flames were reported by Tang et al. (2017), who monitored the size distributions reaching down to 3 nm using an SMPS and DEG SMPS, which were within a factor of 1–5 in the overlapping 3–10 nm region.

Three papers reported comparisons of atmospheric data from mass spectrometers with aerosol measurements in the sub-3 nm size range. Jiang et al. (2011c) reported the first atmospheric neutral cluster comparisons with size distribution measurements starting from 1 nm. While the unit mass resolution of the mass spectrometer introduces considerable uncertainty, the qualitative agreement is relatively good. The DEG SMPS and the SMPS in the size range of 3–10 nm agreed quite well, exhibiting differences of about factor of 1–5. In their comparison of mass-segregated Atmospheric Pressure interface Time of Flight (APi-TSI) data with mobility-segregated, balanced scanning mobility analyzer (BSMA) measurements in a boreal forest environment, Ehn et al. (2011) observed that widening the theoretical transfer function of the BSMA by a factor of 2 significantly improved agreement of the BSMA data with measured ion concentrations. Jen et al. (2015) reported the first laboratory intercomparison of the DEG SMPS with the cluster chemical ionization mass spectrometer (CIMS) using nitrate and acetate ionization. The test aerosol was produced with a flow tube reactor at a range of sulfuric acid and dimethyl amine concentrations. The best agreement between the DEG SMPS and the acetate cluster CIMS was found at high concentrations of dimethyl amine; in general acetate ionization yielded better agreement than did measurements with nitrate ionization. That study demonstrated the challenge of reconciling the mass spectrometric and EMS-based measurements even in controlled laboratory conditions.

Two laboratory comparisons between the PSM and an SMPS have been reported. Kangasluoma et al. (2015b) produced sub-3 nm tungsten trioxide aerosols using a hot-wire generator, and measured the size distributions with the PSM and a Herrmann type DMA-electrometer mobility analyzer system. With careful calibration of both instruments, the agreement was within experimental uncertainties. The fits to the measured distributions agreed within 5%. Cai et al. (2018b) performed a detailed study for the inversion methods of the PSM. They produced a narrow size distribution of tungsten trioxide clusters and sized them with the PSM. The results were compared to a Half-mini DMA-electrometer mobility analyzer system. They found that the inverted concentrations agreed fairly well (within a factor of 1–1.35) for 1.51 nm and 2.41 nm particles, depending on the inversion method. However, at the upper limit of the PSM sizing range, 3.93 nm, the PSM reported significantly lower concentrations with all inversion methods. They also produced a bimodal distribution with peaks around 2 nm and 6 nm. For measurements with the PSM and a HM-based EMS, the inverted concentrations and mode sizes agreed within uncertainties of 20%. Although relatively good agreement was obtained in those laboratory measurements, it is worth noting that during that study, the EMS-based measurements did not include a charge conditioner, thereby eliminating what is likely the greatest source of uncertainty in such measurements.

Two additional laboratory instrument comparisons were presented by Asmi et al. (2009) and Gagne et al. (2011). The former study presented a comparison data from five different NAIS units that were obtained during a single day of measurements of urban air. The size distributions in the 1–10 nm size range agreed within a factor of 2–5. In the latter study, several NAISs were compared against an electrometer or a CPC for size-selected aerosol nanoparticles. The NAIS systems reported concentrations that were higher by a factor of 2–5. They also compared the total concentrations in the size range of 10–40 nm measured by five NAISs with data from a DMPS. Again, the NAISs detected higher concentrations than did the DMPS by a factor of 2–5.

Source-level measurement comparisons reveal even larger differences. Alanen et al. (2015) published size distributions measured in the exhaust of a natural gas engine using both the PSM and a nanoSMPS. While the SMPS detected high concentrations of particles down to 3 nm, the concentrations reported by the PSM were even higher, by a factor of 5–50. Disagreements between the PSM and a nanoSMPS of similar magnitude have been published by Rönkkö et al. (2017) based on measurements of exhaust size distributions at three different engine loads. Xue et al. (2015) used the EEPS and a nanoSMPS to measure exhaust aerosols from different kinds of vehicular sources. They found relatively good agreement between the instruments when the distribution mode diameter was in the 50–100 nm range, but observed much larger disagreement when large number of nucleation mode particles were present.

Arffman et al. (2014) reported laboratory measurements of sub-10 nm dioctylsebacate oil particles with the high-resolution low pressure impactor (HRELPI), a nanoSMPS, a longSMPS and an EEPS. Depending on the input distribution, the disagreement between the instruments varied anywhere from a factor of 1–10, or more; the HRLPI usually reported the highest concentrations.

Dubtsov et al. (2017) operated their diffusion battery in Hyytiälä, and compared the data with that from the NAIS and the DMPS. In the 2.9–6 nm size range, the DMPS showed the lowest particle concentrations, about a factor of ten less than the other two, while the NAIS reported concentrations that were higher than those from the diffusion battery by a factor of 1–4. In the 6–10 nm size range, the DMPS and diffusion battery estimated quite similar particle concentrations, though the DMPS sporadically detected fewer particles. In contrast, the NAIS consistently reported particle concentrations of about a factor of 5 higher.

Some publications have attempted to compare the detailed particle size distributions, but the way that they were presented did not make it easy to assess the level of agreement between the instruments (Alanen et al., 2017; Pinterich et al., 2016). Table 2 summarizes the previous sub-10 nm size distribution measurements in which the size distribution has been measured with at least two independent instruments.

3.4. Synthesis of previous and current sub-10 nm particle size distribution measurements

Based on our review, a few studies exist in which sub-10 nm size distributions were measured and reported based upon data from at least two independent instruments; indeed to our knowledge, only 24 such studies have been reported. This is a relatively small

Table 2
Summary of the instrument comparisons.

Instruments	Test aerosol	Concentration range	Size range [nm]	Factor between the instruments	techniques in order of concentration	Reference
DMPS, Diffusion battery, PHA CPC, Temperature scanning CPC	Arctic air	10^2 - 10^4 [dN/dlogDp]	3–10	1–5	no clear order	Wiedensohler et al. (1994)
DMPS, CPCb, PHA CPC	Boreal forest air	10^2 - 10^4 [dN]	3–10	2 - >10	CPCb > DMPS > PHA CPC	Aalto et al. (2001)
CPCb, NAIS	Boreal forest air	10^2 - 10^4 [dN]	1.8–3	1 - >10	NAIS > CPCb > DMPS	Kulmala et al., 2007
CPCb, NAIS	Boreal forest air	10^2 - 10^4 [dN]	1.5–5	1–10	high conc PHA CPC > NAIS, low conc NAIS > PHA CPC	Lehtipalo et al. (2009)
NAIS	Urban air	10^2 - 10^4 [dN/dlogDp]	2–10	2–5	not applicable	Asmi et al. (2009)
DMPS, NAIS	Boreal forest air	10^2 - 10^4 [dN/dlogDp]	3–40	2 - >10	NAIS > DMPS	Manninen et al. (2009)
PHA CPC, NAIS	Coastal air	10^2 - 10^5 [dN]	1.5–5	1–10	NAIS > PHA CPC	Lehtipalo et al. (2010)
NAIS, DMPS	Urban air	10^2 - 10^4 [dN]	10–40	2–5	NAIS > DMPS	Gagne et al. (2011)
Cluster CIMS, DEG SMPS, SMPS	Urban air	10^3 - 10^7 [dN/dlogDp]	1–10	1–5	DEG SMPS > SMPS, not clear for Cluster CIMS vs DEG SMPS	Jiang et al. (2011c)
DMPS	Urban air	10^2 - 10^4 [dN/dlogDp]	6–10	4 - >10	not applicable	Wiedensohler et al. (2012)
HRLPI, nanoSMPS, longSMPS, EEPS	DOS particles	10^5-10^8 [dN/dlogDp]	4–10	1–10	HRLPI > nanoSMPS > EEPS > longSMPS	Arffman et al. (2014)
PSM, SMPS	WO3	10^4-10^6 [dN/dlogDp]	1.2–2.6	<1.2	no clear order	Kangasluoma et al., 2015
Cluster CIMS, DEG SMPS	Sulfuric acid-DMA	10^6-10^8 [cm-3]	1.23–1.55	1–10	no clear order	Jen et al. (2015)
PSM, DMPS	Engine exhaust	10^5-10^8 [dN/dlogDp]	2–4	5 - >10	PSM > DMPS	Alanen et al. (2015)
EEPS, SMPS	Engine exhaust	10^2-10^6 [dN/dlogDp]	5–10	1 - >10	no clear order	Xue et al. (2015)
vSANC, PSM, DMPS	Boreal forest air	10^1-10^4 [dN/dlogDp]	2–10	?	not possible to infer	Pinterich et al. (2016)
DEG SMPS, SMPS	Flame products	10^8-10^{12} [dN/dlogDp]	3–10	1–5	no clear order	Tang et al. (2017)
DMA train, SMPS	WO3	10^5-10^9 [dN/dlogDp]	1.5–10	1–2	DMA train > SMPS	Stolzenburg et al. (2017)
Diffusion battery, DMPS, NAIS	Boreal forest air	10^2-10^4 [dN]	2.9–10	1 - >10	NAIS > diffusion battery > DMPS	Dubtsov et al. (2017)
PSM, DMPS	Engine exhaust	10^2-10^7 [dN/dlogDp]	1.2–4	5 - >10	PSM > DMPS	Rönkkö et al. (2017)
DMPS, HFDMPS, NAIS	Boreal forest air	10^1-10^4 [dN/dlogDp]	3–10	1.2–10	NAIS > HFDMPS > DMPS	Kangasluoma et al., 2018, this study
PSM, SMPS	WO3	10^3-10^5 [dN/dlogDp]	1.5–4	1–1.35	no clear order	Cai et al., 2018
PSM, NAIS, SMPS	Urban air	10^2-10^5 [dN/dlogDp]	1.2–200	1 - >10	NAIS and PSM > SMPS	This study
PSM, NAIS, DMA train, SMPS, nRDMA	Chamber experiment	10^1-10^5 [dN/dlogDp]	1.3–100	1–10	PSM and NAIS > others	This study

number compared to the amount of research published on sub-10 nm airborne nanoparticles. There is significant room for improvement. Except for the two controlled laboratory experiments where the agreement in the measured distributions was within a factor of 1.5 or less (Cai et al., 2018b; Kangasluoma et al., 2015b), the instrumental disagreement between estimates of the size distribution function spans in the range of 1–10 or more for all of the studies that we have identified. It should be noted that, in the carefully-controlled laboratory experiments, the EMS was operated without a charge conditioner. This removes what may well be the main source of uncertainty in the inverted size distributions.

In some cases, the largest disagreement was observed during measurement periods when one of the instruments showed very low, or zero concentrations. In other cases, large disagreement was observed when one of the instruments is used at its minimum detectable particle size, such as when SMPS/DMPS instruments are used to measure size distributions that include sub-3 nm particles. In the few available studies that present PSM data together with overlapping mobility analyzer measurements, the PSM typically reports higher particle concentrations. However, noting that the PSM and EMSs employ completely different sizing techniques, the qualitative and, sometimes, even the quantitative agreement is good. When sufficient concentrations are available in the 3 nm–10 nm size range, the level of agreement between the measured size distribution functions is more acceptable, generally within a factor of 5 or less. A factor of 5 still represents substantial disagreement considering that the size-resolved particle concentration is one of the most fundamental aerosol properties. In this size range, the NAIS almost always detects the highest size distribution function compared to the other EMSs. These observations indeed highlight the importance of extensive calibrations and instrument comparison workshops, and especially the development of reference methods and absolute, size-resolved particle concentration standards. As a step towards addressing this problem, an ACTRIS calibration facility for sub-10 nm particles and trace gases will be established in Helsinki in the near future.

Because of the simplicity of the CPCb for obtaining particle number concentration over a given size range, closure studies should be put forward under atmospheric conditions that are combined with simulations that take into account the instrument functions. In such an experiment, the integrated concentration in the size range of 1–10 nm from instruments measuring the size distribution will be compared to the concentration measured by a CPCb with a cut-off diameter spanning in the same size range, and the instrument raw signals are simulated by simulating particle size distributions that are "sampled" by the simulated instruments. Only a few such closure studies (without simulations) have been reported even in the super-10 nm size range (Aalto et al., 2001; Covert et al., 1996; Wiedensohler et al. 2012, 2018), while none in the sub-10 nm size range.

Whatever may explain the discrepancies in the measured nanoparticle size distributions, it is crucial for any studies that probe sub-10 nm particles to report measured size distributions, especially in those regions where overlap exists between two or more instruments. This would help to assess the reliability of the subsequent analysis done with the size distributions. Carefully designed and executed experiments that assess the agreement between the different methods under both atmospheric and laboratory conditions, as well as further developments that enhance the agreement between the techniques and instrumental laboratory verifications are in high demand.

4. Measurement uncertainties

The data shown above reveal that major uncertainty exists in measurements of particle size distributions in the low nanometer size regime. In this section, we discuss the sources of uncertainties in sub-10 nm particle measurements according to present understanding. We focus our discussion on the technological issues that directly affect the inversion routines, and on the measurement and inversion accuracy. We consider two major aspects of this uncertainty – concentration accuracy and sizing accuracy – and explore the influence of sampling, charging, sizing, detector cut-off diameter, counting statistics, inversion procedures and the interplay between these aspects of the measurement and data analysis problem. We begin with a general discussion to place these issues into context.

All uncertainties can be considered either random or systematic. Of variables considered here, only counting uncertainty can be considered truly random, as it originates from counting a finite number of objects (particles), and can be described by Poisson statistics that tell whether the expected number of counts in a given time interval is n, the standard deviation for the number actually counted is expected to be $n^{1/2}$. When the counts become small, as they often do in EMS measurements, owing to the low charging probability in the low nanometer size range, the relative uncertainty becomes large. These random effects can often be averaged out by using long averaging times, but that increases the probability that the aerosol being measured will change before the full size distribution is acquired.

Strictly speaking, many other components (charging, CPC cut-off and size distribution related factors) of the uncertainty are systematic at least in the time span of a few minutes during which a size distribution measurement is performed, biasing the measured concentration in a consistent way in a specific system. Over a one year data set, a systematic uncertainty can be treated as random if its magnitude and direction varies randomly within a time scale of e.g. some days or hours. Others may result from sampling different air masses, or the effects of different aerosol sources due to shifts in wind direction and other factors. The aerosol composition may change in the course of a measurement introducing additional, ill-characterized uncertainty. As the magnitude and direction of these uncertainties are typically unknown, they are often treated as random uncertainty, as we do here. Similarly, if no attention is paid to how the sub-10 nm particle sampling is performed, the resulting particle penetration through the sampling line may be close to random.

The sources of systematic uncertainty can be split into three different types: those that introduce constant or size-dependent factors in the inversion procedure (sampling, charging, CPC detection efficiency), poorly defined, but small factors originating from the change of the particle size distribution function over the width of an instrument function (transfer function, kernel function, detection efficiency curve), and incompletely defined, but possibly significant factors affecting the detection efficiency curve of a CPC, such as sample air relative humidity, particle chemical composition and charging state.

Next, these issues are discussed in more detail together with suggested solutions to minimize the uncertainties.

4.1. Concentration accuracy

All of the aforementioned parameters affect the concentration measurement accuracy. The connection between the concentration and sizing accuracy will be discussed in detail in sections 4.4 and 4.5.

4.1.1. Sampling

The first discussed variable is the sampling efficiency that causes uncertainties to the measured size distributions if particle losses that result from diffusion in the sampling lines are not characterized. Particle sampling plays an important role in aerosol characterization, but it is particularly important in measuring sub-3 nm particle concentrations accurately since the losses can be large and variable.

At the inlet of the sampling line, the particle distribution in the tube is generally assumed to be uniform. As the flow is transported along the tube, particles collide with the tube walls due to diffusion and adhere to those walls and are therefore permanently lost from the sample. Those particles closest to the walls are likely to hit the wall first during laminar flow through a straight tube, while the opposite is true for the particles in the flow centerline. This leads eventually to a concentration profile in the tubular flow, in which the smallest concentration is observed close to the walls while the largest concentration in the flow center line (Fu et al., 2019). The longer the residence time in the sampling line, the larger will be the radial gradients in the concentration. If, however, there are bends in the tube, even gentle ones, secondary flows are established that transport particles from the core of the flow to the vicinity of the wall, increasing the particle losses significantly. Turbulent flow at high sampling rates, and high Reynolds numbers, greatly accelerates the transport.

If the particle size distribution is measured downstream of a transport line, the particle losses can be estimated for each size channel separately, while for a total concentration measurement the losses cannot be corrected because the size information is lacking. In the case of sub-3 nm particle sampling, the Gormley & Kennedy equation (Gormley & Kennedy, 1949), which is often used to calculate particle penetration efficiency in tubes, can be considered to give the maximum particle penetration, as any deviations from the cylindrical laminar flow profile, i.e. bends in the tube, changes in tube inner diameter, valves etc. cause local distortions to the flow. Optimally, the sub-10 nm particle sampling lines are always straight tubes with laminar flow. In some special cases where large transport flow rates can be used, turbulent transport can possibly be more efficient than laminar flow transport.

A typical method to estimate particle penetration through complicated tubing is to determine the particle penetration experimentally in the tubing (ratio of size selected particles exiting and entering the tube), and fit an effective length for the penetration vs. particle diameter data using the Gormley & Kennedy equation. Such a method has little theoretical foundation while the fits typically reproduce the observations. Therefore, though being a practical method, the fits have little physical meaning and cannot be reliably extrapolated beyond the range of measurements.

When the flow rate is low or the tube is long, even using only straight tubes with laminar flow for particle transport can easily lead to low penetration through the tubes. Increasing the flow rate in the inlet tube above the instrument inlet flow rate by adding additional transport flow reduces the transport losses of particles. However, the tube connector that is used for creating the transport flow is crucial in determining the losses of the sampling system. The optimal method for creating the transport flow and simultaneously extracting the aerosol flow to the instrument is commonly called the core sampling method. In this method, the sample flow is transported with a larger tube closer to the instrument, and another smaller tube with rounded leading edge is placed in the center line of the larger tube so that it extracts a fraction of the main flow from its center. The flow at the outer edge of the large tube is discarded downstream of the extraction. This configuration extracts the fraction of the flow from which the least particles have diffused to the walls of the transport tube. Using a core sampling system, effective particle transport efficiency can approach 100% even down to 1 nm particle sizes. This is the optimal approach for sub-10 nm particle sampling if one is to minimize the uncertainties: then all particles are transported to the detector with minimal uncertainty in the penetration efficiency. Such a system is analyzed more in detail by Fu et al. (2019), who, in their supplementary material, provide analytical solution with a prepared MATLAB script for designing or characterizing theoretically the core sampling system.

Thus, particle sampling, when conducted and characterized well, should add very little to the concentration measurement uncertainty. As obvious from the previous discussion, traditional aerosol inlets, such as those that incorporate an impactor to minimize sampling of large, multiply-charged particles, valves, diffusion driers, or any other structure in the lines that perturbs the flow, are not suitable for sampling of highly diffusive, sub-10 nm particles.

4.1.2. Charging

A charge conditioner, typically by exposure to bipolar gas ions, brings the aerosols to a steady-state charge distribution. Alternatively, a unipolar charge conditioner may expose the aerosol to ions of a single polarity for a well-defined exposure time. The charge conditioners are usually diffusion-based bipolar radioactive sources and X-ray chargers or unipolar corona needles (Jiang et al., 2014; Mirme & Mirme, 2013; Tigges, Wiedensohler, Weinhold, Gandhi, & Schmid, 2015b; Wiedensohler & Fissan, 1991). The charge conditioners ionize the trace gases in the air and produce ion distributions approximately in the size range of 1–2 nm (Maisser, Thomas, Larriba-Andaluz, He, & Hogan, 2015; Manninen et al., 2011; Steiner et al., 2014), hereafter “charger ions”, which collide and transfer the charge via electrostatically-modified diffusional collisions to the aerosol particles. Most charge conditioners violate the principles outlined above for efficient transmission of nanoparticles. There are also uncertainties related to the approximations in the charging models, and charge distributions may not be uniform and constant inside and downstream of the charger. Therefore, charging may account for a significant fraction of the observed uncertainties in the current EMS measurements.

The fraction of charged particles is a critically important parameter for EMS data inversion, and is probably the main factor limiting

inversion accuracy, especially at sizes close to 1 nm, due to low and poorly characterized charging efficiencies. Usually the charger in EMSs is a radioactive source, of which the resulting charge distribution is often approximated by a parametrization presented by Wiedensohler (1988). However, the charging efficiencies given by the nonphysical polynomial Wiedensohler approximation below at least 5 nm are extrapolations from earlier simulations of Hoppel and Frick (1986) that did not extend to such small sizes (Wiedensohler & Fissan, 1991).

Nowadays, the use of X-ray-based charging is increasing due to strict regulations concerning transportation of radioactive material, even though the bipolar charging using X-ray sources is not completely understood. According to Tigges et al. (2015b), particle charged fractions from an X-ray charger are biased towards higher negatively-charged fractions as compared with the Wiedensohler approximation. Further, the fraction of the charged particles is dependent on the charger ion mobilities and masses (Chen et al., 2018; Chen & Jiang, 2018; Reischl, Mäkelä, Karch, & Necid, 1996) that are rarely known with any accuracy, and vary depending on air composition, impurities and relative humidity (Manninen et al., 2011; Steiner & Reischl, 2012).

This sensitivity can be seen by examining what happens when the ratio of the mobility of positive ions to that of negative ions varies from 0.7 to 1.0, and the ion mobility is in the range from 1 to 2 $cm^2 V^{-1} s^{-1}$. The charge fractions of positively and negatively charged 2 nm particles are estimated to vary over the range of 0.43–1.30% and 0.44–1.35% (Gunn, 1955), respectively. This variation can introduce a factor of 3 uncertainty in the measured concentrations. While few studies have explored the role of particle or ion chemistry on the bipolar charge steady state, chemical properties can be expected to affect the charged fractions in the sub-5 nm size where the particle size approaches few molecules (Premnath et al., 2011). All of these factors make sub-10 nm bipolar charging efficiencies very uncertain and probably dynamic. Recently, a study reported that populations of both positively and negatively charged particles downstream of the bipolar charger can be used to reveal integrated ion properties and subsequently charging efficiencies (Chen et al., 2018; Chen & Jiang, 2018). The sum of positively and negatively-charged particle fractions was shown to be relatively stable under typical conditions and can be adopted by EMSs to reduce the sensitivity to ion properties (Chen et al., 2018). Recently, few studies have addressed some aspects of the charging-related uncertainties, while the Wiedensohler approximation is still widely used (Chen et al., 2018; Chen & Jiang, 2018; Gopalakrishnan, McMurry, & Hogan, 2015; Ibarra, Rodriguez-Maroto, & Alonso, 2019; Leppä, Mui, Grantz, & Flagan, 2017; Lopez-Yglesias & Flagan, 2013; Maisser et al., 2015; Steiner et al., 2014; Tigges et al. 2015a, 2015b). Therefore, more fundamental experimental and theoretical work should be put forward in understanding the charging processes in the sub-10 nm size range and particularly the interplay between the charger ions and the sampled particles under different ionization chemistries and field conditions, and especially on putting the theoretical advances into use in field measurements.

4.1.3. Counting statistics

The two previously mentioned variables, sampling and charging, can be considered as systematic sources of error. Fundamentally random error in the measured concentration originates from CPC counting, of which minimum uncertainty levels can be taken from Poisson statistics. The counting uncertainty resulting from Poisson counting statistics is $\sqrt{N}$, where N is the expected number of raw counts. This uncertainty is the minimum level of random uncertainty, as more randomness can originate from flow fluctuations, changes in the air mass, or many other factors. The counting uncertainty can be easily estimated from the raw counts of the CPC.

Most studies fail to report the absolute number of raw counts in the CPC data in SMPS/DMPS analysis, although a few do (Jiang et al., 2011b; Kangasluoma et al., 2018; Wiedensohler et al., 1994). In the referenced studies, the number of counts measured in polluted Atlanta were below 100 in the 1–3 nm size range, and 100–1000 in the 3–10 nm range. In the more pristine Hyytiälä atmosphere, a conventional ultrafine DMPS recorded counts of 1–20 in 3–10 nm size range, and more specialized DMPS detected about 5–100 particles in the same size range. Thus, in clean environments and in the sub-3 nm size range the counting uncertainties can be significant because of low particle penetration and charging efficiency in the DMPS and SMPS systems. It is unclear to what extent the uncertainties are taken into account in the data inversion software provided by instrument manufacturers, but many report supposedly "raw" CPC data as concentrations rather than counts, making accurate accounting for the statistical uncertainty unlikely.

The only way to minimize counting uncertainties is to increase the number of detected particles in the CPC optics, which in practice means increasing the aerosol flow rate through the optical detector, the counting time or the number of particles reaching the detector from the instrument inlet. For size distribution measurements with an SMPS or DMPS, the aerosol flow rate is an important parameter in defining the detection limit of the instrument and reducing the uncertainties (Cai et al., 2019a). For instance, Kangasluoma et al. (2018) reported 3–5 larger number of detected counts and 50% smaller counting uncertainties for a prototype sub-10 nm DMPS as compared to a long term monitoring DMPS. A significant fraction of these improvements originate from the 3–5 times better counting statistics (aerosol flow rate of 0.05 lpm in TSI 3776 vs 0.71 lpm in Airmodus PSM), with additional improvements due to better sampling efficiency and DMA penetration, but contrary effect from the more narrow transfer function of the DMA. Wiedensohler et al. (1997) and Kangasluoma et al. (2015a) present modifications to the conventional 1 lpm inlet flow rate CPCs that may be used as detectors in SMPS systems even down to 1 nm with increased counting statistics compared to the TSI ultrafine models, though such CPCs are not yet commercially available.

4.1.4. Inversion procedures

The inversion procedures that are used to recover size distributions from the measured counts also introduce uncertainties. In the inversion method for an DMPS, the measured particle size distribution and the overall detection efficiency are often assumed to be constant within the transfer function window (Cai et al., 2019a; Knutson, 1976). However, in the sub-3 nm size range, the shape of size distribution is sometimes steeply sloped (Jiang et al., 2011c). Cai et al. (2019a) reported that for a rising distribution towards a decreasing particle size, the one-to-one inversion method that assumes infinite resolution leads to an uncertainty of up to ~30%.

The performance of an inversion method is also affected by the statistical uncertainties. Compared to the one-to-one inversion

method, the inversion methods considering the size resolution are usually more sensitive to the uncertainties in the raw count number. The one-to-one inversion method assumes that the detection efficiency and size distribution function are constant within the width of the transfer function. Under this assumption, the impact of limited size resolution on the measured signals are neglected, which causes systematic uncertainties. For instance, when the statistical uncertainty of a DMPS measurement is ~15%, the random uncertainties that result from the inversion methods considering the sizing resolution are nearly 5 times that of the total uncertainty of one-to-one method (Cai et al., 2019a; Knutson, 1976; Stolzenburg & McMurry, 2008).

The operation principle of the NAIS is different compared to the DMPS systems because of the electrical detection and unipolar charging, leading to different sources of uncertainty in the inversion procedure. Electrical detection may cause uncertainty at low concentrations, while because of the difficulty in calibrating the charging efficiency, the measured particle concentration have been reported to be overestimated compared with DMPS systems (Gagne et al., 2011; Mirme & Mirme, 2013, see also literature review of this study).

The PSM is a cumulative instrument, for which its inversion procedures differ slightly from the typical EMS inversion. The effect of the inversion methods on the retrieved particle size distributions have been assessed in three previous studies (Cai et al., 2018b; Chan et al., 2020; Lehtipalo et al., 2014). Cai et al. (2018b) demonstrate that, if the original raw data is relatively noiseless, e.g. from stable particle generator, the four examined inversion methods recover the size distribution with up to 30% uncertainty. They also note the possibility of random noise in the measured data increasing the uncertainties during the inversion, which is the case in atmospheric measurements. This was studied by Chan et al. (2020) with measurements in Beijing, who show that during NPF times, the same four inversion methods report quite similar concentrations, a factor of 1.5–2 between minimum and maximum reported concentration. During more polluted times, when the concentration of sub-3 nm particles relative to the total concentration is expected to be low, larger differences between the size distributions recovered from the four inversion methods were observed, and this was especially the case at low sub-3 nm particle concentrations.

4.1.5. Air mass fluctuations

Uncertainty in the measured concentrations can originate from sampled size distribution changes during the course of a single size distribution measurement. Such changes can be due to air mass fluctuations or changes, and can cause significant fluctuations in the inverted concentrations in case there are nearby local particle sources, for example traffic or industrial plants. The changes in the sampled size distributions affect the different measurement methods differently. The effects on the differential methods (e.g., SMPS) are less severe than on the cumulative methods (e.g., PSM, diffusion battery), while methods that measure the whole size distribution simultaneously are the least affected (NAIS, CPCb, DMA train, PHA CPC). For the SMPS, the air mass fluctuations cause fluctuations in the concentrations for individual data points during a single scan, thus the uncertainty is constrained to the data points during which the fluctuations take place. In the PSM and diffusion battery, on the other hand, the inversion of one data point is dependent on the others during the scan, for which strong concentration fluctuations can lead to discarding the whole scan. In the inversion of the instruments that measure the whole size distribution simultaneously, the concentration fluctuations will be averaged during the inversion to the whole size distribution.

4.2. Sizing

The uncertainties in EMS-based measurements' sizing accuracy, and those based on varying the CPC cut-off differ dramatically. Moreover, the sizing accuracy also affects the concentration accuracy, since, especially in the sub-3 nm size, the size distribution can change significantly over the size range of an instrument sizing window (i.e., over the DMA transfer function or CPC cut-off curve). The lower the instrument size resolution, the larger will be the systematic concentration measurement error due to inaccurate sizing, though the method used for data inversion can dramatically affect that sensitivity.

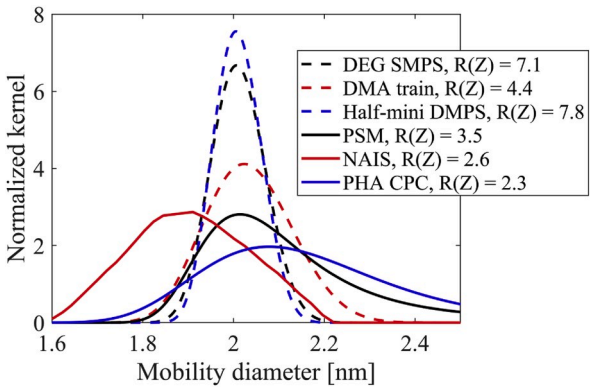

Fig. 6. Kernels normalized by Π and size resolutions (R) of the common instruments used for sub-10 nm size distribution measurements at ~2 nm (Half-mini DMA of the Half-mini DMPS, Cai et al., 2018a; mini cyDMA of the DEG SMPS, Cai et al., 2017a; NAIS, Mirme & Mirme, 2013; PHA CPC, Sipilä et al., 2009; DMA train, Stolzenburg et al., 2017; PSM, Vanhanen et al., 2011).

4.2.1. Size resolution

The definition of the size resolution of a DMA here follows that presented by Flagan (1999): $R = Z/\Delta Z$, where Z is the centroid/peak electrical mobility and ΔZ is the full width at half maximum of the kernel. Fig. 6 visualizes the instrument resolutions and kernels at 2 nm that are normalized by Π. For the EMSs, the kernel widths are governed by the DMA transfer function and they also account for the size dependency of aerosol charge fraction, CPC detection efficiency, and particle diffusion losses inside the instruments. For the PSM, the analogous definition of the kernel at a given size is based upon the derivative of the detection efficiency as a function of the corresponding saturator flow rate of the given size. For the PHA CPC, it is based on the pulse height distributions. Note that the resolution is defined based on Z although in Fig. 6 the kernels are shown as a function of the mobility diameter and the mobility based resolution is approximately half of the resolution with respect to particle mobility diameter. The EMS transfer functions (except for the NAIS, for which transfer function for the channel closest to 2 nm is shown) are relatively symmetric and narrow, suggesting small systematic sizing uncertainties relative to other instruments. For the other instruments, the transfer function is slightly asymmetric and wide. For instance, the concentration at 2 nm detected by the PSM and PHA CPC are affected by the concentration of 2.4 nm particles.

The design and operating conditions of the DMA governs important parameters in the inversion of an EMS: the DMA size resolution in mobility space in the non-diffusive limit is equal to the sheath-to-aerosol flow rate ratio (Flagan, 1999; Knutson & Whitby, 1975). Losses in the entrance region of the DMA reduce total penetration. Electrophoretic losses in the adverse potential gradient at the exit of most DMAs (entrance of the nRDMA) further aggravate those losses. The geometric design further affects the flow laminarity, and determines the useable flow rates, time available for diffusional broadening of the transfer function and particle penetration in the inlet and outlet. In terms of SMPS systems applied to sub-10 nm size distribution measurements, there are several aspects to consider in the design of the DMA, its operating conditions and applications. The traditional Vienna-type DMA or TSI DMAs are limited to around a maximum of 20–40 lpm sheath flow rate, as turbulence develops at larger flow rates (de Juan & Fernandez de la Mora, 1998). This limits their size resolution because of the need to maintain sufficiently high sample flow rate to ensure adequate counting statistics. Fernandez de la Mora et al. (2017) demonstrated a modification to the TSI 3071 DMA sheath flow entrance geometry that allows laminar operation of the DMA up to sheath flow rate of around 100 lpm, reaching a size resolution of around 13 for proteins of 10 nm in diameter. Because of the sheath flow entrance design, flows within the SEADM Half-mini and P5 DMAs have been shown to remain laminar in the classification region up to 1000 lpm, allowing mobility classification with resolution approaching 100 (Amo-Gonzalez & Perez, 2018).

Increasing the sheath flow rate while keeping the aerosol flow rate constant affects the EMS inversion in three ways: it reduces the signal in the detector by narrowing the transfer function; it increases electrostatic losses due to a larger required voltage to classify ions or particles of a fixed mobility, leading to larger electric field in the voltage transition (Attoui & Fernandez de la Mora, 2016; Cai et al., 2019b); and it decreases the systematic sizing error. Extremely large sheath flow rates are mostly useful in laboratory experiments, where the particle concentrations entering the DMA are high enough to obtain sufficient signal in the detector. With atmospheric or other measurements, in which obtaining sufficient signal to the detector is a challenge, the lowest sheath flow rate that still yields sufficient resolution is the optimum solution. A crucial advance in this regard was reported by Fernandéz de la Mora (2017) who improved the aerosol feeding of the Half-mini type DMA with a ring of multiple holes, reducing distortions to the sheath flow at high aerosol-to-sheath flow ratios. This allows use of high aerosol flow rates in SMPS systems utilizing the Half-mini DMA (Cai et al., 2018a). The high voltage required for classification also limits the range of mobilities that can be measured with such high resolution since the maximum voltage is restricted due to the risk of electrostatic breakdown (arcing), so the high flow rate DMAs have found their primary use as calibration sources in the low nanometer size regime, and for use as a mobility precut for mass spectrometric analysis.

4.2.2. CPC cut-off

4.2.2.1. Particle composition and working fluid effect on cut-off. With sub-3 nm CPC calibrations, the most important parameter is the cut-off diameter, which has been shown to be strongly dependent on the chemical effects of the liquid-particle pair (Jiang et al., 2011b; Kangasluoma et al., 2014; Kulmala et al., 2007a; Kupc et al., 2013; Tauber et al., 2019). For minimizing the CPC cut-off related uncertainty, an ideal solution is to calibrate the CPC using particles of the same chemical composition and charging state as the particles of interest. The pulse height distributions in the PHA CPC are also affected by the particle composition (O'Dowd et al., 2004). In practice, for sub-3 nm size range, such calibrations have not yet been conducted for many atmospheric or industrial applications. For atmospheric applications, the efficiency of detection of sulfuric acid particles or sulfuric acid-base clusters may well be close to the calibrations conducted using particles formed when ammonium sulfate is evaporated in a furnace to produce bisulfate clusters with a few ammonia molecules attached to negative polarity clusters (Kangasluoma et al., 2013). This calibration method is quite time consuming not only because of the time required for heating the furnaces, but also because minute quantities of impurities anywhere in the furnace will affect the cluster composition and the results of the calibration. As reported in Kangasluoma et al. (2014), several other calibration compounds, including NaCl, WO_3, $NaNO_3$, and sucrose exhibit quite similar detection efficiency as ammonium sulfate for all CPC working fluids, with cut-off diameters ranging from 1.2 to 1.8 nm for DEG, 1.5–1.9 nm for water, and 1.5–1.8 nm for butanol. Thus, it may be possible to obtain a reasonable calibration for urban aerosols by using some of these compounds. The instrument manufacturers use NaCl (TSI) or CrO_3 (Airmodus) in their instrument verifications.

If the particles of interest consist of hydrocarbons (as in many ambient observations in vegetated areas or urban areas with significant hydrocarbon emissions), obtaining a representative calibration is more challenging than for sulfuric acid systems. Several publications (Jiang et al., 2011b; Kangasluoma et al. 2013, 2014; Kuang, Chen, McMurry, & Wang, 2012; Sipilä et al., 2009; Vanhanen et al., 2011) report that hydrocarbon species are detected with lower efficiencies than other often tested particles. The hydrocarbons

that have been tested including alkylhalide species (Ude & Fernandez de la Mora, 2005), limonene ozonolysis products, and sucrose offer limited experimental data to make general conclusions, though two conclusions can be drawn: the cut-off for hydrocarbons is larger than that for inorganic species. At the onset supersaturation of homogeneous nucleation of DEG, water, and butanol, the cut-off diameters for the tested hydrocarbon aerosol is in the range of 1.8–2.5 nm compared with the range of 1–2 nm for the inorganic test aerosols (Kangasluoma et al., 2014). It should be noted that all these cut-off diameters are subject to experimental uncertainties due to possibly varying amount of impurities in the particles.

The cut-off can be lowered by increasing the supersaturation in the CPC. In the simplest case, when total particle concentration is measured, the CPC d50 can be tuned for any value (in the range of approximately 1.5–10 nm limited by particle losses in the inlet, droplet growth, temperature limits given by the hardware etc.). Lowering the cut-off is limited by the amount of homogeneously-formed droplets, or by the signal-to-noise ratio. Given the small number of counts that are often recorded during SMPS or DMPS measurements, even very low homogenous nucleation rates can seriously degrade the signal-to-noise ratio. Thus, sub-3 nm measurements of hydrocarbon species using the SMPS or DMPS remains a scientific and technological challenge, both in pushing the cut-off closer to 1 nm without homogeneous droplet formation, and in quantifying the size dependent detection efficiency for various organic species.

4.2.3. Particle charge effect on cut-off

Another factor affecting the cut-off at particle size below 3 nm is the particle charging state. Above 3 nm, the charge does not affect the cut-off significantly (Winkler et al., 2008). Practically all CPC calibrations are conducted using charged particles, while most of the measured particles are usually neutral. Only a couple of studies have explored the effect of particle charge state on the CPC cut-off diameter that include also neutral size-selected particles (Kangasluoma et al. 2016b, 2017; Tauber et al., 2019; Winkler et al., 2008). The general finding is that the neutral particles are always detected less efficiently than charged ones, except for NaCl detection by butanol (Tauber et al., 2019). The difference between the charged and neutral cut-off ranges from 0 nm to 0.5 nm, depending on the particle-condensing liquid pair and particle polarity. As shown by Winkler et al. (2008), the charge effect increases with increasing supersaturation or decreasing particle size. Thus, this source of uncertainty is the greatest for the small particles on which this study is focused on. The lack of suitable instrumentation or methods to provide a concentration reference for neutral, sub-3 nm particles, and ways to generate neutral, size-classified sub-3 nm particles of precisely known composition still makes accurate quantification of this problem challenging. The recombination experiments of Steiner et al. (2017), who used two high resolution DMAs to recombine well-characterized ions of opposite polarities, are possibly currently the best method for producing neutral test particles, while not yet applied for instrument characterization.

4.2.4. Cut-off vs concentration

The size dependence of the particle concentration is often strong in systems that produce sub-3 nm particles. Therefore, even a small uncertainty in the CPC cut-off can have a significant effect on the measured size-classified particle concentration. In an SMPS or DMPS measurement, the cut-off uncertainty occurs at the lowest detectable particle size. For scanning Kelvin-effect particle sizing, the detected size distribution function shifts along the diameter axis according to the uncertainty in the cut-offs. Since the size distribution functions can vary strongly within the fractions of nanometers that is the scale of the cut-off uncertainty, the resulting error in the obtained size distribution function can be significant.

When sub-3 nm particles often contribute significantly to the total concentration (Hietikko et al., 2018; Rönkkö et al., 2017), or even dominate it, this uncertainty can also strongly affect the total concentration measurement, for example in near-roadway urban environments. Quantification of the cut-off diameter is one of the most important near future challenges in the sub-3 nm particle measurements. Ideally, alternative sizing mechanisms that are independent of the particle composition should be developed.

Besides the chemical effects of the cut-off to the concentration measurement accuracy, the varying particle concentration also affects the cut-off by vapor depletion and latent heat release due to condensation. Lewis and Hering (2013) demonstrate that the cut-off of a water-based CPC can increase, depending on the geometry, up to 1–8 nm when the particle concentration increases from 0 cm^{-3} to 200 000 cm^{-3}.

4.3. Size resolution vs counting statistics

4.3.1. Limit of detection

The limit of detection (LOD) is the lowest quantity or concentration that can be reliably detected by a given measurement method. The question of what is a reliable measurement varies from field-to-field, and sometimes from one measurement method to another within a given field. The concept is usually applied to measurements of a single quantity, such as the amount of a particular chemical species. Size distributions of aerosols cannot be represented by a single number, and as we have discussed above, the sources of uncertainty vary with particle size and differ dramatically from one method to another. For the SMPS with CPC detection, the LOD has been taken to be the value of the size distribution function corresponding to a single count per channel at the detector. LOD for each given SMPS can be determined through the recently proposed Π parameter. In a brief form, it can be defined as a size dependent constant between the input distribution and instrument response, $\Pi = C/(\mathrm{d}N/\mathrm{dlog}D_p)$, where C is the number of detected counts. Essentially the Π parameter contains the whole instrument function assuming infinite resolution. With this definition, the SMPS LOD ($[\mathrm{d}N/\mathrm{dlog}D_p]$) defined as one count at the CPC is obtained as $\mathrm{LOD} = 1/\Pi$. Given the strong dependence of transmission efficiencies and charging probability with particle size, the LOD, which corresponds to a signal-to-noise ratio (S/N) of unity, increases dramatically with decreasing particle size below 10 nm.

The LOD of the NAIS is determined by the particle concentration that equals the background noise (S/N = 1) based on a 5-min average. The LOD of the PSM is determined as the minimum distinguishable particle concentration at a given concentration of background particles (detected particles that are outside the PSM sizing range). That is, given the background aerosol concentration and the relative uncertainty of the measured particle counts, the LOD of the PSM is equal to its corresponding expected value of the measurement uncertainty (S/N = 1). For PHA CPCs, we define the LOD as the inverted particle concentration from total of 10 counts measured by the multichannel analyzer (MCA). The selected threshold of 10 counts is arbitrary, and the resulting LOD scales linearly with the selected count threshold. The PSM, CPCb and PHA CPC also have LODs for high particle concentration due to the inability of the optics to count individual particles at high particle concentrations due to coincidence errors, usually limited to around 10^5-10^6 cm^{-3}. Further discussion on the LODs can be found from Cai et al. (2019a).

The LOD can be decreased by reducing the instrument resolution, e.g., the DMA transfer function width can be increased by lowering the sheath to aerosol flow rate ratio. A larger number of particles will be detected in the SMPS measurements, and counting uncertainties will be reduced. However, the reduced resolution will increase sizing uncertainties. This challenge can be assessed computationally to find the optimum combination of size resolution and counting statistics as presented by Cai et al. (2019a). We take this method for the uncertainty assessment one step further by incorporating the charging and cut-off related uncertainties into the analysis.

4.3.2. *Full uncertainty assessment*

For a full uncertainty assessment, we ran a Monte Carlo simulation by assuming a bimodal lognormal particle distribution that is representative of a typical aerosol particle distribution during an NPF event. The solid line in Fig. 7a is the one used for the analysis of Fig. 7b-d, the dashed lines are distributions used in Fig. 8 at $dN/d\log D_p = 10^3$, 10^4, 10^5, 10^6 and 10^7.

The procedure to estimate the combined uncertainty (result of all uncertainty components) originating from systematic sizing uncertainty and random counting uncertainty, assumed to be independent of each other, is as follows: the uncertainty due to skewed output distribution because of the finite width of the instrument kernel is obtained from simple multiplication of the size distribution and the kernel. The instrument kernel takes into account all size dependent efficiencies, such as charging and sampling efficiency. The product of the size distribution and the instrument kernel is the measured signal. The obtained signal is inverted using the instrument parameters at the size that is assumed to be classified (e.g. DMA transfer function peak size), and the inverted concentration is compared against the true concentration. This uncertainty can be estimated directly without the Monte Carlo method as it does not include random perturbations.

The random counting uncertainty is estimated by assuming infinite size resolution and simulating the instrument response (number

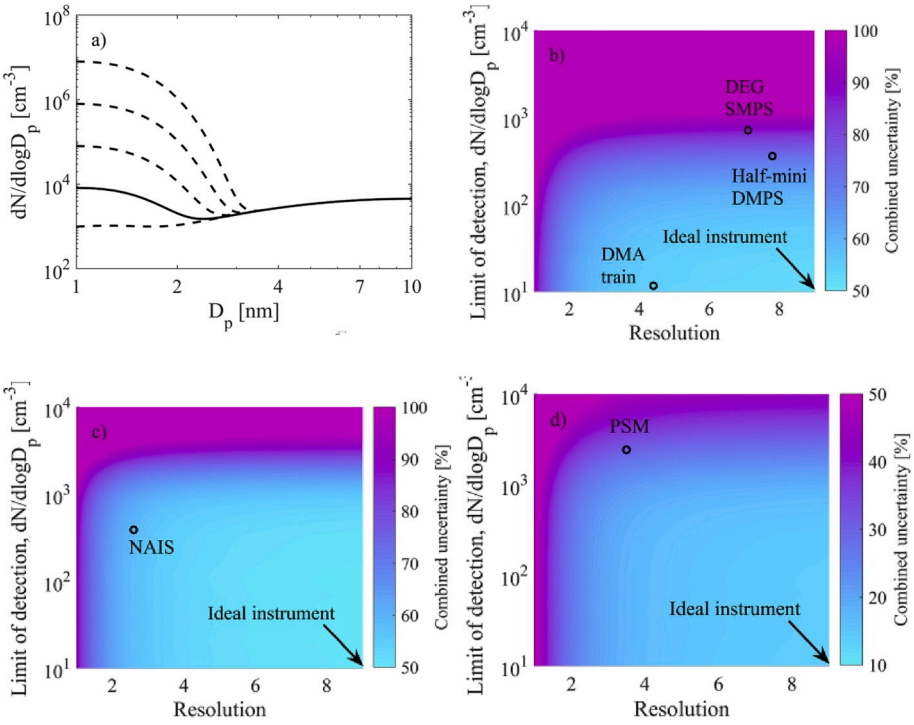

Fig. 7. Analysis of instrument performance for a typical NPF size distribution at 2 nm. Figure a) shows the test distributions, solid line was used for Fig. 7b–d, dashed shows selected distributions used in Fig. 8. Fig 7b shows the uncertainty map for SMPS/DMPS type instruments, 7c for electrometer based ion spectrometers and 7d for Kelvin sizing instruments. Note the different uncertainty color axis in Fig. 7d. (For interpretation of the references to color in this figure legend, the reader is referred to the Web version of this article.)

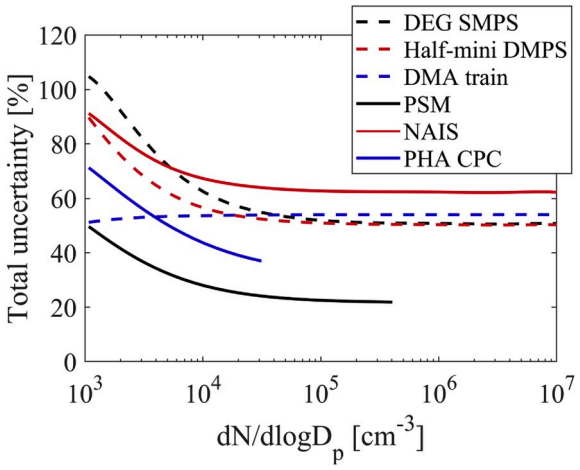

Fig. 8. Instrument uncertainty at 2 nm as a function of the size distribution function peak value. The PSM and PHA CPC lines are cut to approximately represent the highest useable concentration.

of counted particles) obtained from the measurement of the size distribution. At this step the instrument function is perturbed by the assumed uncertainty in the charging efficiency and detection efficiency curve (see next paragraph). The simulated instrument response is perturbed according to Poisson statistics, and the perturbed signal is inverted to size distribution. This simulation is run 10^4 times for each data point, and each time the inverted concentration is compared to the true concentration. The combined uncertainty is the sum of these two uncertainties calculated as the root mean square error (RMS). The LOD vs resolution space covers 1000 points in both directions.

For instrumental parameters, we assume a lognormal distribution around the expected charging efficiency with a geometric standard deviation of 1.65 ($e^{0.5}$) and a normal distribution with a standard deviation of 0.3 nm for the expected value of the CPC cut-off. The charging uncertainty is taken by assuming variation in the product of mean ion mobility (Z) and concentration (C) ratio (Z^+C^+/Z^-C^-) from 0.6 to 1, leading to a charging uncertainty of ±50% (Chen & Jiang, 2018), while the cut-off uncertainty is estimated from Kangasluoma et al. (2014). In practice, for the charging efficiency and cut-off values, we randomly select a value from their corresponding distribution, and calculate the combined uncertainty at 2 nm for each pair of input parameters over the entire LOD vs resolution space. The instruments are subsequently added to the plot based on their LOD and resolution at 2 nm. The Matlab codes to estimate the uncertainties are given in the supplementary material.

Since the cut-off of the CPC of the SMPS and EMS instruments is around 1.3 nm, the cut-off uncertainty does not affect significantly the corresponding combined uncertainty at 2 nm. The problem of cut-offs affecting the concentration detected by the PSM is discussed more in detail by Kangasluoma and Kontkanen (2017) who showed the magnitude of the uncertainties that result when the cut-off uncertainty is directly translated into size distribution function uncertainty. In the following analysis, we do not incorporate the PSM and PHA CPC cut-off uncertainty into the size distribution function uncertainty, but keep in mind that, in addition to the obtained concentration uncertainty, there is uncertainty in the size axis for the PSM and PHA CPC.

Fig. 7b–d presents uncertainties at 2 nm for a typical size distribution that can be observed in rural nucleation events (Fig. 7a), the size distribution function ($dN/d\log D_p$) peak being around 8×10^3 cm^{-3}. The combined uncertainty is plotted as the colored background of Fig. 7b–d. Since the LOD is defined differently for the different types of instruments, calculation of the combined uncertainty is performed separately for the EMS (b), NAIS (c) and PSM (d). The PHA CPC is omitted due to the scarcity of its use. It should be noted that a similar analysis for smaller particles or lower concentrations would result in larger uncertainties, while the uncertainties are smaller for larger particles or concentrations.

The combined uncertainty of the EMSs is in the range of ±50–90%. Due to the better counting statistics obtained by the DMA train compared to the SMPS/DMPS, its uncertainty is smaller. The uncertainty of the PSM is dominated by the background noise, increasing the LOD. At this example concentration, the uncertainty of the SMPS/DMPS instruments would be reduced by better counting statistics, while the uncertainty of DMA train and NAIS is limited by the charging uncertainty. Cai et al. (2019a) previously recommended sizing resolution of 6–8 to be sufficient for atmospheric measurements. This recommendation was based on a distribution similar to the one presented in Fig. 7a that peaks around 10^6, where the slope of the distribution at 2 nm is steeper than in our example, requiring better sizing resolution to reduce the sizing uncertainty.

Table 3 summarizes this analysis. The sampling-related uncertainties are relatively small, or negligible in the case when the sampling lines are well designed, characterized and used. This analysis suggests that charging is one of the main sources of error in the size distribution measurements, but few data exist to estimate the magnitude of the potential error. By observing the trends in the measured 3–10 nm size distributions in both this study and the reviewed papers, the discrepancies most likely originate from some systematic uncertainties, such as charging or instrument calibration. Insufficient size resolution affects the sizing accuracy and causes systematic uncertainty in the range of 5–40% in the measured particle concentration, especially in CPC-based techniques. Systematic sizing errors (which bias the DMA output distribution) lead to concentration errors up to about 5% for the current state-of-the-art SMPS

Table 3
Summary of the concentration and sizing inaccuracy sources.

Source	Physical/chemical source	Affects	Affects	Magnitude	Comment
Unknown line penetration	Diffusion	Concentration	All instruments	Depends on sampling design, negligible if well-designed or characterized, significant for sub-3 nm without characterization	For a size classified particle, linear effect on inverted concentration. Impossible to correct for total concentration measurement
Unknown charging efficiency	Charger ion-particle interactions	Concentration	EMS, DMA train	Highly uncertain, possibly up ±50% relative to Wiedensohler approximation	Linear effect on inverted concentration, can vary in different environments
DMA size resolution	Diffusion, size distribution change over the transfer function width	Concentration, size	EMS, DMA train	Concentration ±0–20%. Size: ±0.5/R % (FWHM of transfer function).	Size uncertainty related to transfer function, concentration uncertainty to systematic sizing error
CPC activation efficiency curve	Vapor-particle interactions/ charge state effects on Kelvin size	Concentration, size	PSM, CPCb, EMS	For concentration: highly system dependent, 0–40%. For sizing: from ±0.1 nm to ±1 nm.	For PSM and CPCb, sizing based on activation efficiency curve accuracy. For EMS, uncertainty of concentration at detection efficiency is affected by activation losses
Counting statistics	Random spatial distribution of particles in air	Concentration	EMS, DMA train	Scales with $\sqrt{N}$, up to ±100% at low concentration	Random effect to inverted concentration
Inversion		Concentration, size	All instruments	Up to ±30%	Depends strongly on size distribution and resolution
Varying size distribution	Air mass changes, nearby local sources	Concentration, size, composition	All instruments	Depends on variations	Complicates PSM inversion more than EMS inversion

systems, while for the lower resolution EMSs the error can be in the range of 5–20%. Error in the sizing due to the CPC cut-off ranges from ±0.1 nm to ±1 nm, depending on the charge state and chemical composition of the measured particles, as well as the supersaturation and composition of the condensing fluid. This sizing error can introduce large uncertainties in the particle concentrations if directly incorporated into the concentration accuracy. Errors originating from low counting statistics most strongly affect EMS measurements in low concentration environments where size distribution functions are below 10^4 cm^{-3}.

In the sub-3 nm size range where PSM data is also available, the absolute concentrations measured by the PSM are likely to be more reliable than those inferred from the EMS inversion. However, as careful instrument calibrations and side by side comparisons are rarely reported together with the measured size distributions, the exact reasons for the observed discrepancies remain ambiguous.

5. Suggestions for selecting instruments

To generalize the analysis above, Fig. 8 presents the estimated combined uncertainty at 2 nm size for the different instruments as a function of the peak concentration in the size distribution; the same parameters, size distribution and charging uncertainty, used in Fig. 7 were used in this estimation, whereas the kernel functions in Fig. 8 are specific to each instrument instead of approximated by normal distributions. In addition, the peak concentration in the size distribution peak was allowed to vary. A second peak in the size distribution at 10 nm diameter was used to represent the background aerosol which was constant at each concentration of the smaller particle mode. The following values are approximate based on the analyzed specific instruments and thus vary from instrument to instrument. It should also be noted that the uncertainties vary as a function of the underlying size distribution; steeper distributions result in larger uncertainties. Therefore, the following discussion should be taken as a general and suggestive guideline for instrument selection and tuning, and the user should consider the characteristics of their own instruments and measurement applications.

At particle concentrations in excess of $dN/d\log D_p = 10^4$ cm^{-3}, the combined uncertainty of around ±50–70% of the EMSs is dominated by the estimated ±50% uncertainty in the particle charging probability; differences between the EMSs at lower concentrations originate from their different sample flow rates, with lower flow rate leading to greater uncertainty. Clearly, the largest improvements would be obtained by reduced uncertainty in the charging of 2 nm particles. The combined uncertainty of the PSM and PHA CPC of around 20–40% derive from the relatively low size resolution, which introduce systematic size biases. It should be noted that the usability of these two methods is limited at high concentrations, for which the line in Fig. 8 is truncated at the approximate maximum concentration. Further, the uncertainties for the PSM increase with increasing concentration due to coincidence or scattering mode detection in the CPC approximately at concentrations above 10^4 cm^{-3}. However, these uncertainties are difficult to generalize and are not depicted in the plot. These concentrations are common to polluted environments such as Beijing, and to some of the laboratory experiments, where similar size distributions were observed (Figs. 3–5). As the number concentration decreases, the combined uncertainties increase because of counting statistics. At $dN/d\log D_p \sim 10^3$ cm^{-3}, as in Hyytiälä (Figs. 1–2), the combined uncertainties range ±50% up to ±100%. Interestingly, the uncertainty of the DMA train decreases with concentration because the background aerosol peak, extending to 2 nm, flattens the size distribution.

For present-day instruments, Fig. 8 suggests: (1) a fundamental understanding of sub-5 nm charging is badly needed, and (2) a good strategy for measurements of particle concentrations of $dN/d\log D_p \sim 10^4$ cm^{-3} or higher would be to optimize the instrument size resolution, while at lower concentrations, the focus should be on maximizing the detected particle counts to improve counting statistics.

The estimated total instrumental uncertainty from this work is similar to, or slightly lower than that suggested by the instrument comparisons in the literature review, and the new size distribution data presented here. These results suggest that our understanding of

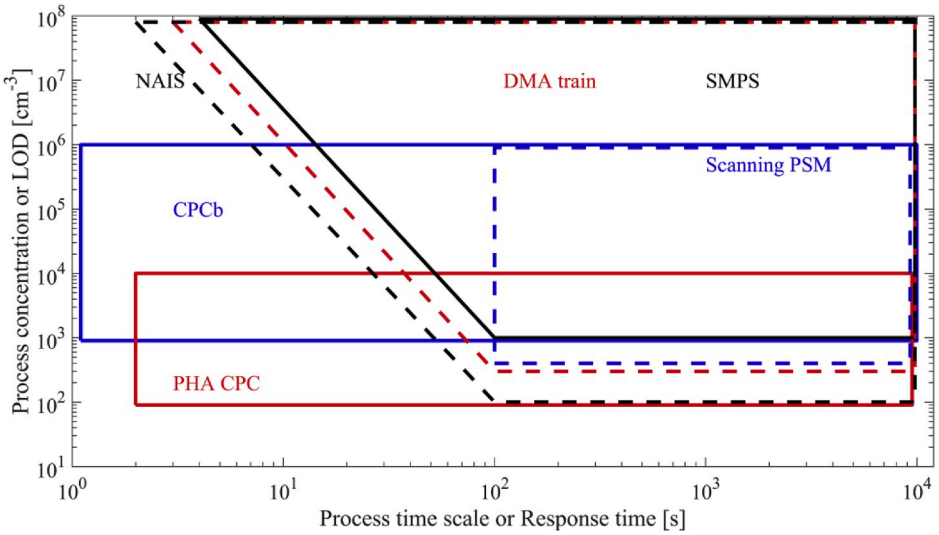

Fig. 9. Instruments classified based on response time and limit of detection.

the measurements and of instrument behavior is quite well captured by the presented uncertainty analysis. Further, the inserted charging uncertainty of ±50% seems reasonable. Disagreement between instruments increases at low concentrations and at decreasing particle size: it may reach a combined uncertainty of ±90%, which translates to about a factor of 20 discrepancy between methods - a level that is often observed in practice.

To visualize the applicability of different instruments for different measurement purposes, Fig. 9 presents instrument LOD or process concentration as a function of the instrument response time or process time scale. Here, we would like to point out that the exact locations of the box borders depend on the instrument settings, while our purpose is to give a general view on the connection of the two presented variables and provide a general level discussion.

The CPCb LOD is low as it is only based on the subtraction of two concentration measurements; this method also has an upper concentration limit due to coincidence errors. The CPCb has time resolution in the order of 1 s, which is mostly limited by the CPC and its sampling line response time. Thus, CPCb is suitable for most applications, except for measurements of extremely high concentrations, such as those found in some industrial processes or exceptionally polluted areas. The method's size resolution is limited by the number of CPCs employed.

The PHA CPC is a rarely-utilized technique, which in principle should have a time resolution of 1 s and a relatively low detection limit. According to reports on butanol-based PHA CPCs (Sipilä et al., 2009), the response of the PHA CPC is affected by large particle concentrations, which limits its applicability at high concentration environments. However, this limitation might be overcome by use of some other working fluids, while it has not been explored yet.

Some of the mobility analyzer methods can attain response times down to a few seconds. The highest response times for the EMSs are estimations based on the instrument characteristics, and lowest LODs are estimated based on Π values at 2 nm from Cai et al. (2019a). Very fast scans using a DMA are possible, but commercially-available detectors degrade measurement accuracy by skewing of the detected size distribution due to slow CPC response times. Moreover, counting statistics may be poor due to the short counting times that can be tolerated during fast scans. A detailed analysis of this problem is missing from the literature. Typically, the SMPS measurements employ scans of a few minutes, leading to LODs of about 10^2-10^3 cm^{-3}. An exception is the DMA train, which has an even lower LOD because its DMAs sit at fixed voltage, increasing the counting statistics significantly compared to scanning EMSs. The response time of the DMA train type instruments is in the range of some seconds, likely limited by the flow smearing in the transport lines and the response time of the CPC.

The present scanning-mode PSM is set to scan from minimum to maximum supersaturation in 2 min. Because of this, the PSM should be used with care to characterize processes of which characteristic timescales are less than 2 min. The LOD of the PSM is similar to that of the CPCb or the DMA train, while it is also limited at large concentrations due to the CPC-based detection method.

The presented analysis shows that present day instruments cover the LOD vs response-time map very well. The most immediate gaps in the instrumentation are possibly 1 s measurements of extremely high concentrations, or sub-1 s measurements. These could be possibly done with a CPCb, although it requires very careful characterization of the system response time. Also, the CPCb can be constructed from available commercial instruments, while no ready-made commercial CPCb solutions exist.

6. Summary and conclusions

In this overview, we studied the previous literature in which sub-10 nm particle number size distribution measurements using at least two independent instruments, presented new size distribution data from three sites, and showed that the current size distribution measurements are subject to uncertainties that are larger than previously suggested. Due to these uncertainties, significant discrepancies exist in the observed size distributions between the instruments, especially during times of relatively low concentrations. Depending on the measurement method, the lowest and highest reported particle concentrations in the critical sub-10 nm size range can vary by a factor of 1–10 or more. Discrepancies tend to be the highest when one of the instruments detects low concentrations, or is near its detection limit. From the present uncertainty assessment, we estimate this factor to be about maximum of 2–4 for concentrations above 10^4, and 3–20 for concentrations below 10^4, suggesting our analysis captures the observed deviations between the size distribution functions reported in the literature quite well. Generally, in the size range between 3 and 10 nm, the NAIS reports the largest concentrations, while SMPS systems report the lowest. In the sub-3 nm size range, the PSM generally observes higher concentrations compared with mobility analyzers. Overall, the general trends observed in the size distribution agree quite well, while some systematic discrepancies are included in the obtained particle size distributions, of which sources remain ambiguous.

We have discussed six separate sources for uncertainty for the measurements of sub-10 nm size distributions: particle transport losses, charging efficiency, DMA sizing, CPC cut-off, particle counting, and inversion uncertainty. Of these, the combined total uncertainties are likely dominated by the charge distribution for mobility sizing devices; the CPC cut-off size and signal fluctuation related uncertainty are also important and dominant for Kelvin sizing instruments. Particle transport losses can be efficiently minimized by using the core sampling system, while uncharacterized and/or poorly designed sampling lines can lead to significant particle losses. Uncertainty in particle concentration due non-flat size distribution and to the assumption of zero width for the instrument transfer function or detection efficiency curves are limited to maximum of around 5–20% with present instruments.

We can conclude:

- There is still considerable amount of scientific work remaining to improve the sub-10 nm particle size distribution measurement accuracy, especially in the low nanometer size regime.

- Charging is the major source of uncertainty in mobility analysis because of the unknown interplay between the charger ion properties and charged fractions, especially in the low nanometer and near micrometer regimes. Moreover, the charging probability may vary from one charge conditioner to another, and even over time within the same unit.
- Charging and the diffusive transfer functions are likely the major sources of uncertainty in the NAIS. Future efforts should focus on the particle mode measurement accuracy and calibration.
- Composition effects on activation are the greatest sources of uncertainty in Kelvin effect sizing; concentration is also a factor affecting pulse-height analysis, but also likely in the PSM and CPCb due to coincidence at much higher concentrations.
- Counting statistics are also an important source of uncertainty in the DMPS/SMPS measurements especially in the sub-5 nm size range, which could be easily estimated and reported from the CPC counts

From our analysis, we can identify several advances that are needed to improve the accuracy and widen the applicability of the size distribution measurements below 10 nm:

- Several advances are needed. Systematic, rigorous calibration, routine calibration validation exercises during deployment, and the development of traceable references and standards for size and concentration should be developed to ensure that measurements are accurate.
- As evident from the literature review, only a few efforts have been published in which different particle sizing techniques are calibrated first, and then compared side-by-side. Such experiments, would give more information on the performance of the different techniques.
- The supersaturation scan technique should be optimized both in terms of time resolution and size range. Especially increasing the size range from the current 1–3 nm range would increase its usability.
- For characterizing fast industrial processes and mobile measurements, employing CPC batteries are good solution while currently no clear commercial options are available.
- Compared with other mobility analyzers, the NAIS has limited size resolution and uses a unipolar charger; this leads to high uncertainties in the reported data. The next steps in the development of the NAIS should focus on the inversion, size resolution and absolute size-resolved particle concentration accuracy.
- Fundamental research should be put forward to understand charging efficiencies and to reduce the variability of CPC cut-off with the particle chemical composition. These would tremendously reduce particle concentration measurement uncertainties as well as increase data comparability.
- Specialized CPCs with high aerosol flow rate and supersaturation would reduce counting uncertainties and LOD of SMPS/DMPS systems.

Acknowledgements

We are indebted for the anonymous reviewer for the extensive, insightful and detailed reviews. This work was supported by UHEL Faculty of Science support grant (75284140) and 3-year grant (75284132), Finnish Academy of Science projects (1325656, 1306853 and 1296628), Academy of Finland Center of Excellence in Atmospheric Sciences (272041), ERC Grant NANODYNAMITE (616075), ERC grant ATM-GTP (742206), National Key R&D Program of China (2017YFC0209503), National Science Foundation of China (21876094), Pusan National University Research Grant, 2018, National Research Foundation of Korea (NRF-2019R1F1A1058854), and the European Union's Horizon 2020 research and innovation programme under grant agreement No 654109 and previously from the European Union Seventh Framework Programme (FP7/2007–2013) under grant agreement n° 262254.

Appendix A. Supplementary data

Code for the uncertainty estimations can be found online at https://doi.org/10.1016/j.jaerosci.2020.105584.

References

Aalto, P., Hameri, K., Becker, E., Weber, R., Salm, J., Makela, J. M., et al. (2001). Physical characterization of aerosol particles during nucleation events. *Tellus B: Chemical and Physical Meteorology, 53*, 344–358.

Agarwal, J. K., & Sem, G. J. (1980). Continuous flow, single-particle-counting condensation nucleus counter. *Journal of Aerosol Science, 11*, 343–357.

Ahonen, L. R., Kangasluoma, J., Lammi, J., Lehtipalo, K., Hameri, K., Petaja, T., et al. (2017). First measurements of the number size distribution of 1-2nm aerosol particles released from manufacturing processes in a cleanroom environment. *Aerosol Science & Technology, 51*, 685–693.

Airmodus. https://airmodus.com/wp-content/uploads/2018/09/a11ncnc_datasheet_180530.pdf. Read 7.11.2019.

Alanen, J., Saukko, E., Lehtoranta, K., Murtonen, T., Timonen, H., Hillamo, R., et al. (2015). The formation and physical properties of the particle emissions from a natural gas engine. *Fuel, 162*, 155–161.

Alanen, J., Simonen, P., Saarikoski, S., Timonen, H., Kangasniemi, O., Saukko, E., et al. (2017). Comparison of primary and secondary particle formation from natural gas engine exhaust and of their volatility characteristics. *Atmospheric Chemistry and Physics, 17*, 8739–8755.

Amo-Gonzalez, M., & Perez, S. (2018). Planar differential mobility analyzer with a resolving power of 110. *Analytical Chemistry, 90*, 6735–6741.

Arffman, A., Juuti, P., Harra, J., & Keskinen, J. (2017). Differential diffusion analyzer. *Aerosol Science & Technology, 51*, 1429–1437.

Arffman, A., Yli-Ojanpera, J., Kalliokoski, J., Harra, J., Pirjola, L., Karjalainen, P., et al. (2014). High-resolution low-pressure cascade impactor. *Journal of Aerosol Science, 78*, 97–109.

Asmi, E., Sipila, M., Manninen, H. E., Vanhanen, J., Lehtipalo, K., Gagne, S., et al. (2009). Results of the first air ion spectrometer calibration and intercomparison workshop. *Atmospheric Chemistry and Physics, 9*, 141–154.
Attoui, M., & Fernandez de la Mora, J. (2016). Flow driven transmission of charged particles against an axial field in antistatic tubes at the sample outlet of a Differential Mobility Analyzer. *Journal of Aerosol Science, 100*, 91–96.
Bartz, H., Fissan, H., Helsper, C., Kousaka, Y., Okuyama, K., Fukushima, N., et al. (1985). Response characteristics for 4 different condensation nucleus counters to particles in the 3-50 Nm diameter range. *Journal of Aerosol Science, 16*, 443–456.
Betrancourt, C., Liu, F. S., Desgroux, P., Mercier, X., Faccinetto, A., Salamanca, M., et al. (2017). Investigation of the size of the incandescent incipient soot particles in premixed sooting and nucleation flames of n-butane using LII, HIM, and 1 nm-SMPS. *Aerosol Science & Technology, 51*, 916–935.
Bricard, J., Delattre, P., Madelaine, G., & Pourprix, M. (1976). Detection of ultra-fine particles by means of a continuous flux condensation nuclei counter. In *Fine particles* (pp. 565–580). New York: Academic Press.
ten Brink, H. M., Plomp, A., Spoelstra, H., & Vandevate, J. F. (1983). A high-resolution electrical mobility aerosol spectrometer (mas). *Journal of Aerosol Science, 14*, 589–597.
Brunelli, N. A., Flagan, R. C., & Giapis, K. P. (2009). Radial differential mobility analyzer for one nanometer particle classification. *Aerosol Science & Technology, 43*, 53–59.
Buckley, D. T., & Hogan, C. J. (2017). Determination of the transfer function of an atmospheric pressure drift tube ion mobility spectrometer for nanoparticle measurements. *Analyst, 142*, 1800–1812.
Cai, R., Attoui, M., Jiang, J., Korhonen, F., Hao, J., Petäjä, T., et al. (2018a). Characterization of a high-resolution supercritical differential mobility analyzer at reduced flow rates. *Aerosol Science & Technology, 52*, 1332–1343.
Cai, R., Chen, D. R., Hao, J., & Jiang, J. (2017a). A miniature cylindrical differential mobility analyzer for sub-3 nm particle sizing. *Journal of Aerosol Science, 106*, 111–119.
Cai, R., Jiang, J., Mirme, S., & Kangasluoma, J. (2019a). Parameters governing the performance of electrical mobility spectrometers for measuring sub-3 nm particles. *Journal of Aerosol Science, 127*, 102–115.
Cai, R., Yang, D., Ahonen, L. R., Shi, L., Korhonen, F., Petäjä, T., et al. (2018b). Data inversion methods to determine sub-3 nm aerosol size distributions using the Particle Size Magnifier. *Atmos Meas Tech, 11*, 4477–4491.
Cai, R. L., Yang, D. S., Fu, Y. Y., Wang, X., Li, X. X., Ma, Y., et al. (2017b). Aerosol surface area concentration: A governing factor in new particle formation in beijing. *Atmospheric Chemistry and Physics, 17*, 12327–12340.
Cai, R., Zhou, Y., & Jiang, J. (2019b). Transmission of charged nanoparticles through the DMA adverse axial electric field and its improvement. *Aerosol Science & Technology, 54*, 21–32.
Chan, T., Cai, R., Ahonen, L. R., Liu, Y., Zhou, Y., Vanhanen, J., et al. (2020). Assessment of particle size magnifier inversion methods to obtain particle size distribution from atmospheric measurements. *Atmospheric Measurement Techniques Discussions*. https://doi.org/10.5194/amt-2019-465.
Chen, X., & Jiang, J. (2018). Retrieving the ion mobility ratio and aerosol charge fractions for a neutralizer in real-world applications. *Aerosol Science & Technology, 52*, 1145–1155.
Chen, X., McMurry, P., & Jiang, J. (2018). Stationary characteristics in bipolar diffusion charging of aerosols: Improving the performance of electrical mobility size spectrometers. *Aerosol Science & Technology, 52*, 809–813.
Chen, D. R., Pui, D. Y. H., Hummes, D., Fissan, H., Quant, F. R., & Sem, G. J. (1998). Design and evaluation of a nanometer aerosol differential mobility analyzer (Nano-DMA). *Journal of Aerosol Science, 29*, 497–509.
Covert, D., Wiedensohler, A., Aalto, P., Heintzenberg, J., McMurry, P., & Leck, C. (1996). Aerosol number size distributions from 3 to 500 nm diameter in the arctic marine boundary layer during summer and autumn. *Tellus B: Chemical and Physical Meteorology, 48*, 197–212.
Dick, W. D., McMurry, P. H., Weber, R. J., & Quant, F. R. (2000). White-light detection for nanoparticle sizing with the TSI ultrafine condensation particle counter. *Journal of Nano Research, 2*, 85–90.
Dubtsov, S., Ovchinnikova, T., Valiulin, S., Chen, X., Manninen, H. E., Aalto, P. P., et al. (2017). Laboratory verification of Aerosol Diffusion Spectrometer and the application to ambient measurements of new particle formation. *Journal of Aerosol Science, 105*, 10–23.
Duplissy, J., Enghoff, M. B., Aplin, K. L., Arnold, F., Aufmhoff, H., Avngaard, M., et al. (2010). Results from the CERN pilot CLOUD experiment. *Atmospheric Chemistry and Physics, 10*, 1635–1647.
Ehn, M., Junninen, H., Schobesberger, S., Manninen, H. E., Franchin, A., Sipila, M., et al. (2011). An instrumental comparison of mobility and mass measurements of atmospheric small ions. *Aerosol Science & Technology, 45*, 522–532.
Eisele, F. L., & Tanner, D. J. (1993). Measurement of the gas-phase concentration of H2so4 and methane sulfonic-acid and estimates of H2so4 production and loss in the atmosphere. *Journal of Geophysical Research - D: Atmospheres, 98*, 9001–9010.
Erikson, H. A. (1921). The change of mobility of the positive ions in air with age. *Phys. Rev., 18*, 100–101.
Fernandéz de la Mora, J. (2017). Expanded flow rate range of high-resolution nanoDMAs via improved sample flow injection at the aerosol inlet slit. *Journal of Aerosol Science, 113*, 265–275.
Fernandez de la Mora, J., & Barrios-Collado, C. (2017a). A bipolar electrospray source of singly charged salt clusters of precisely controlled composition. *Aerosol Science & Technology, 51*, 778–786.
Fernandez de la Mora, J., Gao, P., & Perez-Lorenzo, L. J. (2017b). Eliminating the main source of instability and turbulence in TSI's 3071 DMA. *Aerosol Science & Technology, 51*, 896–902.
Fernandez de la Mora, J., Hering, S. V., Rao, N., & McMurry, P. H. (1990). Hypersonic impaction of ultrafine particles. *Journal of Aerosol Science, 21*, 169–187.
Fernandéz de la Mora, J., & Kozlowski, J. (2013). Hand-held differential mobility analyzers of high resolution for 1-30 nm particles: Design and fabrication considerations. *Journal of Aerosol Science, 57*, 45–53.
Fiebig, M., Stein, C., Schröder, F., Feldpausch, P., & Petzold, A. (2005). Inversion of data containinginformation on the aerosol particle size distribution usingmultiple instruments. *Journal of Aerosol Science, 36*, 1353–1372.
Fissan, H. J., Helsper, C., & Thielen, H. J. (1983). Determination of particle-size distributions by means of an electrostatic classifier. *Journal of Aerosol Science, 14*, 354–357.
Flagan, R. C. (1998). History of electrical aerosol measurements. *Aerosol Science & Technology, 28*, 301–380.
Flagan, R. (1999). On differential mobility analyzer resolution. *Aerosol Science & Technology, 30*, 556–570.
Flagan, R. C., Wang, S. C., Yin, F., Seinfeld, J. H., Reischl, G., Winklmayr, W., et al. (1991). Electrical mobility measurements of fine-particle formation during chamber studies of atmospheric photochemical reactions. *Environmental Science & Technology, 25*, 883–890.
Franchin, A., Downard, A., Kangasluoma, J., Nieminen, T., Lehtipalo, K., Steiner, G., et al. (2016). A new high-transmission inlet for the Caltech nano-RDMA for size distribution measurements of sub-3 nm ions at ambient concentrations. *Atmos Meas Tech, 9*, 2709–2720.
Fuchs, N. A. (1962). On the determination of particle size distribution in polydisperse aerosols by the diffusion method. *British Journal of Applied Physics, 13*, 280.
Fuchs, N. A. (1963). On the stationary charge distribution on aerosol particles in a bipolar ionic atmosphere. *Geofis. Pura Appl., 56*, 185–193.
Fu, Y., Xue, M., Cai, R., Kangasluoma, J., & Jiang, J. (2019). Theoretical and experimental analysis of the core sampling method: Reducing diffusional losses in aerosol sampling line. *Aerosol Science & Technology, 53*, 793–801.
Gagne, S., Lehtipalo, K., Manninen, H. E., Nieminen, T., Schobesberger, S., Franchin, A., et al. (2011). Intercomparison of air ion spectrometers: An evaluation of results in varying conditions. *Atmos Meas Tech, 4*, 805–822.
Gamero-Castano, M., & Fernandéz de la Mora, J. (2000). A condensation nucleus counter (CNC) sensitive to singly charged sub-nanometer particles. *Journal of Aerosol Science, 31*, 757–772.
Gerdien, H. (1903). Die absolute Messung der elektrischen Leitfahigkeit und der spezifischen lonengeschwindigkeit in der atmosphare. *Physikalische Zeitschrift, 4*, 632–635.

Gopalakrishnan, R., McMurry, P. H., & Hogan, C. J. (2015). The bipolar diffusion charging of nanoparticles: A review and development of approaches for non-spherical particles. *Aerosol Science & Technology, 49*, 1181–1194.
Gormley, P. G., & Kennedy, M. (1949). Diffusion from a stream flowing through a cylindrical tube. *Proceedings of the Royal Irish Academy - Section A: Mathematical and Physical Sciences, 52*, 163–169.
Gunn, R. (1955). The statistical electrification of aerosols by ionic diffusion. *Journal of Colloid and Interface Science, 10*, 107–119.
Hari, P., & Kulmala, M. (2005). Station for measuring ecosystem-atmosphere relations (SMEAR II). *Boreal Environment Research, 10*, 315–322.
Hering, S. V., Stolzenburg, M. R, Quant, F. R., Oberreit, D. R., & Keady, P. B. (2005). A Laminar-Flow, Water-Based Condensation Particle Counter (WCPC). *Aerosol Science and Technology, 39*(7), 659–672. https://doi.org/10.1080/02786820500182123.
Hering, S. V., Fernandez de la Mora, J., & Halpern, B. L. (1988). Performance of an opposed-jet molecular impactor with W(Co)6 molecules suspended in a H-2 carrier gas. *Aerosol Science & Technology, 8*, 1–9.
Hering, S. V., Lewis, G. S., Spielman, S. R., Eiguren-Fernandez, A., Kreisberg, N. M., Kuang, C., et al. (2017). Detection near 1-nm with a laminar-flow, water-based condensation particle counter. *Aerosol Science & Technology, 51*.
Hietikko, R., Kuuluvainen, H., Harrison, R. M., Portin, H., Timonen, H., Niemi, J. V., et al. (2018). Diurnal variation of nanocluster aerosol concentrations and emission factors in a street canyon. *Atmospheric Environment, 189*, 98–106.
Hoppel, W. A., & Frick, G. M. (1986). Ion aerosol attachment coefficients and the steady-state charge-distribution on aerosols in a bipolar ion environment. *Aerosol Science & Technology, 5*, 1–21.
Ibarra, I., Rodriguez-Maroto, J., & Alonso, M. (2019). Bipolar charging and neutralization of particles below 10 nm, the conditions to reach the stationary charge distribution, and the effect of a non-stationary charge distribution on particle sizing. *Journal of Aerosol Science*. https://www.sciencedirect.com/science/article/pii/S002185021930583X.
Iida, K., Stolzenburg, M. R., & McMurry, P. H. (2009). Effect of working fluid on sub-2 nm particle detection with a laminar flow ultrafine condensation particle counter. *Aerosol Science & Technology, 43*, 81–96.
Jen, C. N., Hanson, D. R., & McMurry, P. H. (2015). Toward reconciling measurements of atmospherically relevant clusters by chemical ionization mass spectrometry and mobility classification/vapor condensation. *Aerosol Science & Technology, 49*, I–Iii.
Jiang, J. K., Attoui, M., Heim, M., Brunelli, N. A., McMurry, P. H., Kasper, G., et al. (2011a). Transfer functions and penetrations of five differential mobility analyzers for sub-2 nm particle classification. *Aerosol Science & Technology, 45*, 480–492.
Jiang, J. K., Chen, M. D., Kuang, C. A., Attoui, M., & McMurry, P. H. (2011b). Electrical mobility spectrometer using a diethylene glycol condensation particle counter for measurement of aerosol size distributions down to 1 nm. *Aerosol Science & Technology, 45*, 510–521.
Jiang, J. K., Kim, C. M., Wang, X. L., Stolzenburg, M. R., Kaufman, S. L., Qi, C. L., et al. (2014). Aerosol charge fractions downstream of six bipolar chargers: Effects of ion source, source activity, and flowrate. *Aerosol Science & Technology, 48*, 1207–1216.
Jiang, J. K., Zhao, J., Chen, M. D., Eisele, F. L., Scheckman, J., Williams, B. J., et al. (2011c). First measurements of neutral atmospheric cluster and 1-2 nm particle number size distributions during nucleation events. *Aerosol Science & Technology, 45*(ii-V).
Johnson, T., Caldow, R., Pöcher, A., Mirme, A., & Kittelson, D. (2004). *A new electrical mobility particle sizer spectrometer for engine exhaust particle measurements*. SAE Technical paper 2004-01-1341.
Jokinen, T., Sipila, M., Junninen, H., Ehn, M., Lonn, G., Hakala, J., et al. (2012). Atmospheric sulphuric acid and neutral cluster measurements using CI-APi-TOF. *Atmospheric Chemistry and Physics, 12*, 4117–4125.
de Juan, L., & Fernandez de la Mora, J. (1998). High resolution size analysis of nanoparticles and ions: Running a Vienna DMA of near optimal length at Reynolds numbers up to 5000. *Journal of Aerosol Science, 29*, 617–626.
Junninen, H., Ehn, M., Petaja, T., Luosujarvi, L., Kotiaho, T., Kostiainen, R., et al. (2010). A high-resolution mass spectrometer to measure atmospheric ion composition. *Atmos Meas Tech, 3*, 1039–1053.
Kangasluoma, J., Ahonen, L., Attoui, M., Vuollekoski, H., Kulmala, M., & Petaja, T. (2015a). Sub-3nm particle detection with commercial TSI 3772 and Airmodus A20 fine condensation particle counters. *Aerosol Science & Technology, 49*, 674–681.
Kangasluoma, J., Ahonen, L. R., Laurila, T., Cai, R., Enroth, J., Mazon, S., et al. (2018). Laboratory verification of a new high flow differential mobility particle sizer, and field measurements in Hyytiälä. *Journal of Aerosol Science, 124*, 1–9.
Kangasluoma, J., & Attoui, M. (2019). Review of sub-3 nm condensation particle counters, calibrations, and cluster generation methods. *Aerosol Science & Technology, 53*, 1277–1310.
Kangasluoma, J., Attoui, M., Junninen, H., Lehtipalo, K., Samodurov, A., Korhonen, F., et al. (2015b). Sizing of neutral sub 3 nm tungsten oxide clusters using Airmodus Particle Size Magnifier. *Journal of Aerosol Science, 87*, 53–62.
Kangasluoma, J., Franchin, A., Duplissy, J., Ahonen, L., Korhonen, F., Attoui, M., et al. (2016a). Operation of the Airmodus A11 nano Condensation Nucleus Counter at various inlet pressures and various operation temperatures, and design of a new inlet system. *Atmos Meas Tech, 9*, 2977–2988.
Kangasluoma, J., Hering, S., Picard, D., Lewis, G., Enroth, J., Korhonen, F., et al. (2017). Characterization of three new condensation particle counters for sub-3 nm particle detection during the Helsinki CPC workshop: The ADI versatile water CPC, TSI 3777 nano enhancer and boosted TSI 3010. *Atmos Meas Tech, 10*, 2271–2281.
Kangasluoma, J., Junninen, H., Lehtipalo, K., Mikkila, J., Vanhanen, J., Attoui, M., et al. (2013). Remarks on ion generation for CPC detection efficiency studies in sub-3-nm size range. *Aerosol Science & Technology, 47*, 556–563.
Kangasluoma, J., & Kontkanen, J. (2017). On the sources of uncertainty in the sub-3 nm particle concentration measurement. *Journal of Aerosol Science, 112*, 34–51.
Kangasluoma, J., Kuang, C., Wimmer, D., Rissanen, M. P., Lehtipalo, K., Ehn, M., et al. (2014). Sub-3 nm particle size and composition dependent response of a nano-CPC battery. *Atmos Meas Tech, 7*, 689–700.
Kangasluoma, J., Samodurov, A., Attoui, M., Franchin, A., Junninen, H., Korhonen, F., et al. (2016b). Heterogeneous nucleation onto ions and neutralized ions: Insights into sign-preference. *Journal of Physical Chemistry C, 120*, 7444–7450.
Kerminen, V. M., Paramonov, M., Anttila, T., Riipinen, I., Fountoukis, C., Korhonen, H., et al. (2012). Cloud condensation nuclei production associated with atmospheric nucleation: A synthesis based on existing literature and new results. *Atmospheric Chemistry and Physics, 12*, 12037–12059.
Keskinen, J., Pietarinen, K., & Lehtimäki, M. (1992). Electrical low pressure impactor. *Journal of Aerosol Science, 23*, 353–360.
Kim, C. S., Okuyama, K., & de la Mora, J. F. (2003). Performance evaluation of an improved particle size magnifier (PSM) for single nanoparticle detection. *Aerosol Science & Technology, 37*, 791–803.
Kim, T., Suh, S. M., Girshick, S. L., Zachariah, M. R., McMurry, P. H., Rassel, R. M., et al. (2002). Particle formation during low-pressure chemical vapor deposition from silane and oxygen: Measurement, modeling, and film properties. *Journal of Vacuum Science and Technology A, 20*, 413–423.
Kirkby, J., Curtius, J., Almeida, J., Dunne, E., Duplissy, J., Ehrhart, S., et al. (2011). Role of sulphuric acid, ammonia and galactic cosmic rays in atmospheric aerosol nucleation. *Nature, 476*, 429–U477.
Knutson, E. O. (1976). Extended electric mobility method for measuring aerosol particle size and concentration. In B. Y. H. Liu (Ed.), *Fine particles: Aerosol generation, measurement, sampling, and analysis* (pp. 739–762). New York, NY: Academic Press.
Knutson, E. O., & Whitby, K. T. (1975). Aerosol classification by electric mobility: Apparatus, theory and applications. *Journal of Aerosol Science, 6*, 443–451.
Kontkanen, J., Lehtipalo, K., Ahonen, L., Kangasluoma, J., Manninen, H. E., Hakala, J., et al. (2017). Measurements of sub-3nm particles using a particle size magnifier in different environments: From clean mountain top to polluted megacities. *Atmospheric Chemistry and Physics, 17*, 2163–2187.
Krechmer, J. E., Groessl, M., Zhang, X., Junninen, H., Massoli, P., Lambe, A., et al. (2016). Ion mobility spectrometry–mass spectrometry (IMS–MS) for on and offline analysis of atmospheric gas and aerosol species. *Atmos Meas Tech, 9*, 3245–3262.
Kuang, C. (2018). A diethylene glycol condensation particle counter for rapid sizing of sub-3nm atmospheric clusters. *Aerosol Science & Technology, 10*, 1112–1119.
Kuang, C. A., Chen, M. D., McMurry, P. H., & Wang, J. (2012). Modification of laminar flow ultrafine condensation particle counters for the enhanced detection of 1 nm condensation nuclei. *Aerosol Science & Technology, 46*, 309–315.

Kulmala, M., Mordas, G., Petaja, T., Gronholm, T., Aalto, P. P., Vehkamaki, H., et al. (2007a). The condensation particle counter battery (CPCB): A new tool to investigate the activation properties of nanoparticles. *Journal of Aerosol Science, 38*, 289–304.
Kulmala, M., Riipinen, I., Sipila, M., Manninen, H. E., Petaja, T., Junninen, H., et al. (2007b). Toward direct measurement of atmospheric nucleation. *Science, 318*, 89–92.
Kupc, A., Bischof, O., Tritscher, T., Beeston, M., Krinke, T., & Wagner, P. E. (2013). Laboratory characterization of a new nano-water-based CPC 3788 and performance comparison to an ultrafine butanol-based CPC 3776. *Aerosol Science & Technology, 47*, 183–191.
Lehtipalo, K., Kulmala, M., Sipila, M., Petaja, T., Vana, M., Ceburnis, D., et al. (2010). Nanoparticles in boreal forest and coastal environment: A comparison of observations and implications of the nucleation mechanism. *Atmospheric Chemistry and Physics, 10*, 7009–7016.
Lehtipalo, K., Leppa, J., Kontkanen, J., Kangasluoma, J., Franchin, A., Wimnner, D., et al. (2014). Methods for determining particle size distribution and growth rates between 1 and 3 nm using the Particle Size Magnifier. *Boreal Environment Research, 19*, 215–236.
Lehtipalo, K., Sipila, M., Riipinen, I., Nieminen, T., & Kulmala, M. (2009). Analysis of atmospheric neutral and charged molecular clusters in boreal forest using pulse-height CPC. *Atmospheric Chemistry and Physics, 9*, 4177–4184.
Leppä, J., Mui, W., Grantz, A. M., & Flagan, R. (2017). Charge distribution uncertainty in differential mobility analysis of aerosols. *Aerosol Science & Technology, 51*, 1168–1189.
Lewis, G. S., & Hering, S. (2013). Minimizing concentration effects in water-based, laminar-flow condensation particle counters. *Aerosol Science & Technology, 47*, 645–654.
Liu, J., Jiang, J., Zhang, Q., Deng, J., & Hao, J. (2016). A spectrometer for measuring particle size distributions in the range of 3 nm to 10 μm. *Frontiers of Environmental Science & Engineering, 10*, 63–72.
Liu, B. Y. H., & Pui, D. Y. H. (1975). On the performance of the electrical aerosol analyzer. *Journal of Aerosol Science, 6*, 249–254.
Lopez-Yglesias, X., & Flagan, R. C. (2013). Ion-aerosol flux coefficients and the steady-state charge distribution of aerosols in a bipolar ion environment. *Aerosol Science & Technology, 47*, 688–704.
Mai, H. J., Kong, W. M., Seinfeld, J. H., & Flagan, R. C. (2018). Scanning DMA data analysis II. Integrated DMA-CPC instrument response and data inversion. *Aerosol Science & Technology, 52*, 1400–1414.
Maisser, A., Thomas, J. M., Larriba-Andaluz, C., He, S., & Hogan, C. J. (2015). The mass–mobility distributions of ions produced by a Po-210 source in air. *Journal of Aerosol Science, 90*, 36–50.
Mäkelä, J., Aalto, P., Jokinen, V., Pohja, T., Nissinen, A., Palmroth, S., et al. (1997). Observations of ultrafine aerosol particle formation and growth in boreal forest. *Geophysical Research Letters, 24*, 1219–1222.
Manninen, H. E., Franchin, A., Schobesberger, S., Hirsikko, A., Hakala, J., Skromulis, A., et al. (2011). Characterisation of corona-generated ions used in a neutral cluster and air ion spectrometer (NAIS). *Atmos Meas Tech, 4*, 2767–2776.
Manninen, H. E., Petaja, T., Asmi, E., Riipinen, I., Nieminen, T., Mikkila, J., et al. (2009). Long-term field measurements of charged and neutral clusters using Neutral cluster and Air Ion Spectrometer (NAIS). *Boreal Environment Research, 14*, 591–605.
Marti, J. J., Weber, R. J., Saros, M. T., Vasiliou, J. G., & McMurry, P. H. (1996). Modification of the TSI 3025 condensation particle counter for pulse height analysis. *Aerosol Science & Technology, 25*, 214–218.
McMurry, P. H. (2000). The history of condensation nucleus counters. *Aerosol Science & Technology, 33*, 297–322.
Merikanto, J., Spracklen, D. V., Mann, G. W., Pickering, S. J., & Carslaw, K. S. (2009). Impact of nucleation on global CCN. *Atmospheric Chemistry and Physics, 9*, 8601–8616.
Mirme, S., & Mirme, A. (2013). The mathematical principles and design of the NAIS - a spectrometer for the measurement of cluster ion and nanometer aerosol size distributions. *Atmos Meas Tech, 6*, 1061–1071.
Mirme, A., Tamm, E., Mordas, G., Vana, M., Uin, J., Mirme, S., et al. (2007). A wide-range multi-channel air ion spectrometer. *Boreal Environment Research, 12*, 247–264.
Mordas, G., Sipila, M., & Kulmala, M. (2008). Nanometer particle detection by the condensation particle counter UF-02proto. *Aerosol Science & Technology, 42*, 521–527.
O'Dowd, C., Aalto, P. P., Yoon, Y. J., & Hämeri, K. (2004). The use ofthe pulse height analyser ultrafine condensation particle counter (PHA-UCPC) technique applied to sizing ofnucleation mode particles of differing chemical composition. *Journal of Aerosol Science, 35*, 205–216.
Oberreit, D. R., McMurry, P. H., & Hogan, C. J. (2014a). Analysis of heterogeneous uptake by nanoparticles via differential mobility analysis-drift tube ion mobility spectrometry. *Physical Chemistry Chemical Physics, 16*, 6968–6979.
Oberreit, D. R., McMurry, P. H., & Hogan, C. J. (2014b). Mobility analysis of 2 nm to 11 nm aerosol particles with an aspirating drift tube ion mobility spectrometer. *Aerosol Science & Technology, 48*, 108–118.
Oberreit, D., Rawat, V. K., Larriba-Andaluz, C., Ouyang, H., McMurry, P. H., & Hogan, C. J. (2015). Analysis of heterogeneous water vapor uptake by metal iodide cluster ions via differential mobility analysis-mass spectrometry. *The Journal of Chemical Physics, 143*.
Okuyama, K., Kousaka, Y., & Motouchi, T. (1984). Condensational growth of ultrafine aerosol-particles in a new particle-size magnifier. *Aerosol Science & Technology, 3*, 353–366.
Olenius, T., Pichelstorfer, L., Stolzenburg, D., Winkler, P. M., Lehtinen, K. E. J., & Riipinen, I. (2018). Robust metric for quantifying the importance of stochastic effects on nanoparticle growth. *Sci Rep-Uk, 8*.
Ouyang, H., He, S. Q., Larriba-Andaluz, C., & Hogan, C. J. (2015). IMS-MS and IMS-IMS investigation of the structure and stability of dimethylamine-sulfuric acid nanoclusters. *The Journal of Physical Chemistry A, 119*, 2026–2036.
Petäjä, T., Sipilä, M., Paasonen, P., Nieminen, T., Kurten, T., Ortega, I. K., et al. (2011). Experimental observation of strongly bound dimers of sulfuric acid: Application to nucleation in the atmosphere. *Physical Review Letters, 106*.
Pinterich, T., Vrtala, A., Kaltak, M., Kangasluoma, J., Lehtipalo, K., Petaja, T., et al. (2016). The versatile size analyzing nuclei counter (vSANC). *Aerosol Science & Technology, 50*, 947–958.
Premnath, V., Oberreit, D., & Hogan, C. J. (2011). Collision-based ionization: Bridging the gap between chemical ionization and aerosol particle diffusion charging. *Aerosol Science & Technology, 45*, 712–726.
Reischl, G. P., Mäkelä, J. M., Karch, R., & Necid, J. (1996). Bipolar charging of ultrafine particles in the size range below 10 nm. *Journal of Aerosol Science, 27*, 931–949.
Rohmann, H. (1923). Methode sur Messung der Grosse von Schwebeteilchen. *Zeitschrift für Physik, 17*, 253–265.
Rönkkö, T., Kuuluvainen, H., Karjalainen, P., Keskinen, J., Hillamo, R., Niemi, J. V., et al. (2017). Traffic is a major source of atmospheric nanocluster aerosol. *P Natl Acad Sci USA, 114*, 7549–7554.
Saros, M. T., Weber, R. J., Marti, J. J., & McMurry, P. H. (1996). Ultrafine aerosol measurement using a condensation nucleus counter with pulse height analysis. *Aerosol Science & Technology, 25*, 200–213.
Seto, T., Okuyama, K., de Juan, L., & Fernandéz de la Mora, J. (1997). Condensation of supersaturated vapors on monovalent and divalent ions of varying size. *Journal of Physical Chemistry, 107*, 1576–1585.
Sgro, L. A., & Fernandéz de la Mora, J. (2004). A simple turbulent mixing CNC for charged particle detection down to 1.2 nm. *Aerosol Science & Technology, 38*, 1–11.
Sinclair, D., & Hoopes, G. S. (1975). A continuous flow condensation nucleus counter. *Journal of Aerosol Science, 6*, 1–7.
Sipilä, M., Lehtipalo, K., Attoui, M., Neitola, K., Petaja, T., Aalto, P. P., et al. (2009). Laboratory verification of PH-CPC's ability to monitor atmospheric sub-3 nm clusters. *Aerosol Science & Technology, 43*, 126–135.
Sipilä, M., Lehtipalo, K., Kulmala, M., Petaja, T., Junninen, H., Aalto, P. P., et al. (2008). Applicability of condensation particle counters to measure atmospheric clusters. *Atmospheric Chemistry and Physics, 8*, 4049–4060.
Smith, J. N., Moore, K. F., McMurry, P. H., & Eisele, F. L. (2004). Atmospheric measurements of sub-20 nm diameter particle chemical composition by thermal desorption chemical ionization mass spectrometry. *Aerosol Science & Technology, 38*, 100–110.

Spracklen, D. V., Carslaw, K. S., Kulmala, M., Kerminen, V. M., Sihto, S. L., Riipinen, I., et al. (2008). Contribution of particle formation to global cloud condensation nuclei concentrations. *Geophysical Research Letters, 35*.
Steiner, G., Franchin, A., Kangasluoma, J., Kerminen, V. M., Kulmala, M., & Petaja, T. (2017). Production of neutral molecular clusters by controlled neutralization of mobility standards. *Aerosol Science & Technology, 51*, 946–955.
Steiner, G., Jokinen, T., Junninen, H., Sipila, M., Petaja, T., Worsnop, D., et al. (2014). High-resolution mobility and mass spectrometry of negative ions produced in a Am-241 aerosol charger. *Aerosol Science & Technology, 48*, 261–270.
Steiner, G., & Reischl, G. P. (2012). The effect of carrier gas contaminants on the charging probability of aerosols under bipolar charging conditions. *Journal of Aerosol Science, 54*, 21–31.
Stolzenburg, M. R., & McMurry, P. H. (1991). An ultrafine aerosol condensation nucleus counter. *Aerosol Science & Technology, 14*, 48–65.
Stolzenburg, M. R., & McMurry, P. H. (2008). Equations governing single and tandem DMA configurations and a new lognormal approximation to the transfer function. *Aerosol Science & Technology, 42*, 421–432.
Stolzenburg, M. R., Scheckman, J. H. T., Attoui, M., Han, H. S., & McMurry, P. H. (2018). Characterization of the TSI model 3086 differential mobility analyzer for classifying aerosols down to 1nm. *Aerosol Science & Technology, 52*, 748–756.
Stolzenburg, D., Steiner, G., & Winkler, P. M. (2017). A DMA-train for precision measurement of sub-10 nm aerosol dynamics. *Atmos Meas Tech, 10*, 1639–1651.
Tammet, H. (2006). Continuous scanning of the mobility and size distribution of charged clusters and nanoparticles in atmospheric air and the Balanced Scanning Mobility Analyzer BSMA. *Atmospheric Research, 82*, 523–535.
Tammet, H. (2011). Symmetric inclined grid mobility analyzer for the measurement of charged clusters and fine nano- particles in atmospheric air. *Aerosol Science & Technology, 45*, 468–479.
Tammet, H., Mirme, A., & Tamm, E. (2002). Electrical aerosol spectrometer of tartu university. *Atmospheric Research, 62*, 315–324.
Tang, Q., Cai, R., You, X., & Jiang, J. (2017). Nascent soot particle size distributions down to 1 nm from a laminar premixed burner-stabilized stagnation ethylene flame. *Proceedings of the Combustion Institute, 36*, 993–1000.
Tauber, C., Brilke, S., Wlasits, P. J., Bauer, P. S., Koberl, G., Steiner, G., et al. (2019). Humidity effects on the detection of soluble and insoluble nanoparticles in butanol operated condensation particle counters. *Atmos Meas Tech, 12*, 3659–3671.
Tigges, L., Jain, A., & Schmid, H. J. (2015a). On the bipolar charge distribution used for mobility particle sizing: Theoretical considerations. *Journal of Aerosol Science, 88*, 119–134.
Tigges, L., Wiedensohler, A., Weinhold, K., Gandhi, J., & Schmid, H. J. (2015b). Bipolar charge distribution of a soft X-ray diffusion charger. *Journal of Aerosol Science, 90*, 77–86.
Tröstl, J., Tritscher, T., Bischof, O. F., Horn, H. G., Krinke, T., Baltensperger, U., et al. (2015). Fast and precise measurement in the sub-20 nm size range using a Scanning Mobility Particle Sizer. *Journal of Aerosol Science, 87*, 75–87.
TSI https://www.tsi.com/getmedia/d0b7d247-37bc-4584-93be-d3a0b2a7141a/1nm-SMPS-3938E57_US_5002241_RevA_WEB?ext=.pdf. Read 7.11.2019.
Ude, S., & Fernandez de la Mora, J. (2005). Molecular monodisperse mobility and mass standards from electrosprays of tetra-alkyl ammonium halides. *Journal of Aerosol Science, 36*, 1224–1237.
Vanhanen, J., Mikkila, J., Lehtipalo, K., Sipila, M., Manninen, H. E., Siivola, E., et al. (2011). Particle size magnifier for nano-CN detection. *Aerosol Science & Technology, 45*, 533–542.
Wang, S. C., & Flagan, R. C. (1990). Scanning electrical mobility spectrometer. *Aerosol Science & Technology, 13*, 230–240.
Wang, Y., Kangasluoma, J., Attoui, M., Fang, J., Junninen, H., Kulmala, M., et al. (2017). The high charge fraction of flame-generated particles in the size range below 3 nm measured by enhanced particle detectors. *Combustion and Flame, 176*, 72–80.
Wang, J., McNeill, V. F., Collins, D. R., & Flagan, R. C. (2002). Fast mixing condensation nucleus counter: Application to rapid scanning differential mobility analyzer measurements. *Aerosol Science & Technology, 36*, 678–689.
Wehner, B., Werner, F., Ditas, F., Shaw, R. A., Kulmala, M., & Siebert, H. (2015). Observations of new particle formation in enhanced UV irradiance zones near cumulus clouds. *Atmospheric Chemistry and Physics, 15*, 11701–11711.
Wiedensohler, A. (1988). An approximation of the bipolar charge distribution for particles in the submicron size range. *Journal of Aerosol Science, 19*, 387–389.
Wiedensohler, A., Aalto, P., Covert, D., Heintzenberg, J., & McMurry, P. (1994). Intercomparison of four methods to determine size distributions of low-concentration (~ 100 cm-3), ultrafine aerosols ($3 < D p < 10$ nm) with illustrative data from the arctic. *Aerosol Science & Technology, 21*, 95–109.
Wiedensohler, A., Birmili, W., Nowak, A., Sonntag, A., Weinhold, K., Merkel, M., et al. (2012). Mobility particle size spectrometers: Harmonization of technical standards and data structure to facilitate high quality long-term observations of atmospheric particle number size distributions. *Atmos Meas Tech, 5*, 657–685.
Wiedensohler, A., & Fissan, H. (1991). Bipolar charge distributions of aerosol particles in high-purity argon and nitrogen. *Aerosol Science & Technology, 14*, 358–364.
Wiedensohler, A., Orsini, D., Covert, D. S., Coffmann, D., Cantrell, W., Havlicek, M., et al. (1997). Intercomparison study of the size-dependent counting efficiency of 26 condensation particle counters. *Aerosol Science & Technology, 27*, 224–242.
Wiedensohler, A., Wiesner, A., Weinhold, K., Birmili, W., Hermann, M., Merkel, M., et al. (2018). Mobility particle size spectrometers: Calibration procedures and measurement uncertainties. *Aerosol Science & Technology, 52*, 146–164.
Wimmer, D., Lehtipalo, K., Franchin, A., Kangasluoma, J., Kreissl, F., Kurten, A., et al. (2013). Performance of diethylene glycol-based particle counters in the sub-3 nm size range. *Atmos Meas Tech, 6*, 1793–1804.
Winkler, P. M., Steiner, G., Vrtala, A., Vehkamaki, H., Noppel, M., Lehtinen, K. E. J., et al. (2008). Heterogeneous nucleation experiments bridging the scale from molecular ion clusters to nanoparticles. *Science, 319*, 1374–1377.
Winkler, P. M., Vrtala, A., Wagner, P. E., Kulmala, M., Lehtinen, K. E. J., & Vesala, T. (2004). Mass and thermal accommodation during gas-liquid condensation of water. *Physical Review Letters, 93*.
Winklmayr, W., Reischl, G. P., Lindner, A., & Berner, A. (1991). A new electromobility spectrometer for the measurement of aerosol size distributions in the size range from 1 to 1000 nm. *Journal of Aerosol Science, 22*, 289–296.
Wu, J. J., Cooper, D. W., & Miller, R. J. (1989). Evaluation of aerosol deconvolution algorithms for determining sub-micron particle-size distributions with diffusion battery and condensation nucleus counter. *Journal of Aerosol Science, 20*, 477–482.
Xue, J., Wang, X., Durbin, T. D., Johnson, K. C., Karavalakis, G., Asa-Awuku, A., et al. (2015). Comparison of vehicle exhaust particle size distributions measured by SMPS and EEPS during steady-state conditions. *Aerosol Science & Technology, 49*, 984–996.
Yao, L., Garmash, O., Bianchi, F., Zheng, J., Yan, C., Kontkanen, J., et al. (2018). Atmospheric new particle formation from sulfuric acid and amines in a Chinese megacity. *Science, 361*, 278–281.
Zeleny, J. (1900). The velocity of the ions produced in gases by rongten rays. *Phil. Trans. Roy. Soc. A., 195*, 193–234.
Zhao, J., Eisele, F. L., Titcombe, M., Kuang, C. G., & McMurry, P. H. (2010). Chemical ionization mass spectrometric measurements of atmospheric neutral clusters using the cluster-CIMS. *Journal of Geophysical Research - D: Atmospheres, 115*.
Zhou, Y., Dada, L., Liu, Y., Fu, Y., Kangasluoma, J., Chan, T., et al. (2019). Variation of size-segregated particle number concentrations in winter Beijing. *Atmospheric Chemistry and Physics, 20*, 1201–1216.